medications nor AChE inhibitors other than donepezil before the PET study. All patients met the National Institute of Neurological and Communicative Disorders and Stroke-Alzheimer's Disease and Related Disorders Association criteria for probable AD.[20] The absence of focal cerebral abnormalities was confirmed by magnetic resonance imaging in all the patients.

This study was approved by the institutional review board of the National Institute of Radiological Sciences, Chiba, Japan. Written informed consent was obtained from each participant and/or his/her caregiver in the family before the study.

Calculation of Donepezil-Induced Inhibition of Cortical AChE Activity Using [^{11}C]MP4A PET

We performed [^{11}C]MP4A PET in 16 patients with probable AD in the baseline PET studies. The patients started to receive donepezil orally at a dose of 3 mg once a day for 2 weeks after the baseline PET study, followed by 5 mg daily for 5.3 ± 2.0 (mean ± SD) months until the second PET study. The patients took 5 mg of donepezil at 8 AM and underwent the follow-up PET study at 3 PM. All medications other than donepezil were withdrawn at least 12 hours before the PET study. A venous blood sample was obtained from each patient with AD for the measurement of the plasma concentration of donepezil around 3 PM just before tracer injection in the second PET study.

A sequence of 14 PET scan was acquired with EXACT 47 scanner (Siemens/CTI, Knoxville, Tenn) covering 40 minutes after IV injection of [^{11}C]MP4A (approximately 740 MBq) in each subject. Twenty-four arterial blood samples were collected at the predetermined intervals for 15 minutes after IV tracer injection for measurement of total radioactivity and metabolite analysis. A three-compartment model was used to yield estimation of K_1 (transport into tissue), k_2 (tissue clearance of unchanged tracer into blood), and k_3 (hydrolysis rate of [^{11}C]MP4A by AChE, ie, AChE activity) using metabolite-corrected arterial plasma input function. The voxel-by-voxel k_3 value was calculated with the arterial input function. The procedures in detail were previously described.[9,13,21] The voxels of interest were automatically determined in the bilateral frontal cortex (superior frontal gyrus and middle frontal gyrus), sensorimotor cortex (precentral and postcentral gyrus), temporal cortex (superior temporal gyrus), parietal cortex (inferior parietal gyrus), occipital cortex (middle occipital gyrus and cuneus), and in the posterior cingulate cortex using the analytic software, the voxel-based stereotactic extraction estimation, which determines anatomical information in respective brain coordinates[22] with the Talairach Daemon.[23] The regional cortical k_3 values and donepezil-induced inhibition rates were calculated. Percentage changes in k_3 value were defined by the following formula:

$$\%\ \text{change in}\ k_3 = \left(k_{3(b)} - k_{3(f)}\right) / k_{3(b)} \times 100$$

where $k_{3(f)}$ and $k_{3(b)}$ represent k_3 values at the time of follow-up and at baseline, respectively. Data in the striatum and cerebellum were not analyzed because k_3 estimates in these brain regions with high AChE activity are not reliable because of the characteristics of this technique.[9]

Estimation of Plasma IC_{50}

A venous blood sample was taken from each patient with AD for measurement of plasma concentration of donepezil just before tracer injection (around 3 PM) in the second PET study. The plasma components were separated immediately from the cellular components by centrifugation and stored at -20°C until the analysis. Plasma concentrations were measured using a specific and sensitive high-performance liquid chromatography method with ultraviolet detection. The lowest quantifiable concentration was 2.0 ng/mL.[24,25] We investigated the correlation between plasma donepezil concentrations and AChE inhibition rates in the cerebral cortex. Then, the value of in vivo plasma IC_{50} of donepezil, that is, the concentration of donepezil in plasma that inhibits brain AChE activity by 50% at the steady-state conditions of donepezil between the plasma and the brain, was calculated by measurement of plasma donepezil concentrations and the cerebral cortical AChE inhibition rates evaluated with [^{11}C]MP4A PET. The plasma IC_{50} was estimated using a simple one-parameter model as followed:

$$\text{AChE inhibition} = [\text{I}]/(\text{plasma}\ IC_{50} + [\text{I}])$$

where AChE inhibition represents mean k_3 reduction in the cortical voxels of interest defined above and [I] represents the donepezil concentration in the plasma.[17,26,27] The standard errors of plasma IC_{50} estimates were calculated with the variance-covariance matrix.

RESULTS

The steady-state plasma concentration of donepezil after oral doses of 5 mg/day was 28.9 ± 7.3 ng/mL after 5.3 ± 2.0 months of treatment in patients with AD. The inhibition levels of AChE activity in cerebral cortices caused by donepezil are shown in Table 1. The plasma concentration of donepezil ranged from 18.5 to 43.9 ng/mL with mean of 28.9 ± 7.3 ng/mL, and the inhibition rates of the cerebral cortical AChE activity ranged from 21.0% to 43.6% with mean of 34.6 ± 7.3% compared with those in the baseline study ($P < 0.0001$). The AChE activity was uniformly inhibited by donepezil among cortical regions as in the lateral temporal cortex (37.1%), followed by superior frontal (35.4%), sensorimotor (35.1%), posterior cingulate (33.1%), occipital (32.5%), and parietal (32.4%) cortices.

The plasma IC_{50} value estimated from plasma donepezil concentrations and the cerebral cortical mean AChE inhibition rates measured by PET was 53.6 ± 4.0 ng/mL (Fig. 1). The correlation between the plasma donepezil concentration and the AChE inhibition rate remained 0.50 ($P = 0.05$).

DISCUSSION

The PET evaluation provides unique information on the in vivo pharmacology of AChE inhibitors and novel drugs. Until the development of a PET technique for the measurement of

TABLE 1. The Regional Cortical k_3 Values (Mean ± SD) and Donepezil-Induced Inhibition Rate Measured by [^{11}C]MP4A PET

Region	k_3 (per minute)		Inhibition (%)
	Pretreatment	Posttreatment	
Frontal	0.0674 ± 0.0075	0.0433 ± 0.0058	35.4 ± 8.6*
Sensorimotor	0.0744 ± 0.0089	0.0481 ± 0.0069	35.1 ± 7.5*
Lateral temporal	0.0695 ± 0.0096	0.0435 ± 0.0074	37.1 ± 8.2*
Parietal	0.0566 ± 0.0077	0.0388 ± 0.0057	32.4 ± 8.6*
Occipital	0.0543 ± 0.0067	0.0365 ± 0.0053	32.5 ± 7.7*
Posterior cingulate	0.0584 ± 0.0062	0.0388 ± 0.0049	33.1 ± 9.9*
Cortical mean	0.0634 ± 0.0065	0.0414 ± 0.0055	34.6 ± 7.3*

Data are expressed as mean ± SD.

[^{11}C]MP4A indicates *N*-[^{11}C] methylpiperidin-4-yl acetate.

*$P < 0.0001$: significant reduction against pretreatment (2-tailed paired *t* test).

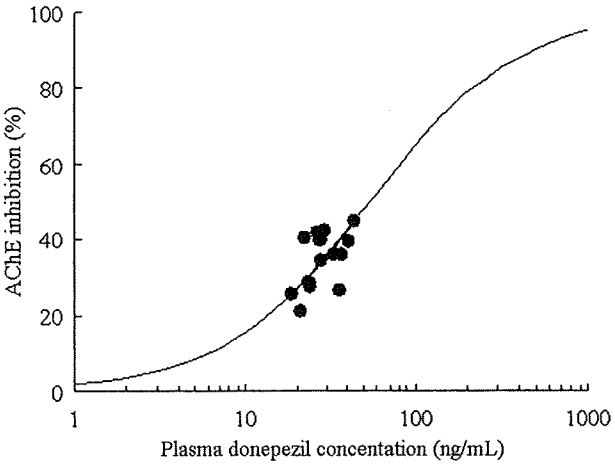

FIGURE 1. Relationship between the plasma donepezil concentration and the percentage inhibition of brain AChE activity. According to the concentration-inhibition curve, the plasma IC50 value of donepezil is estimated at 53.6 ± 4.0 ng/mL (approximately 130 nM). Using the reported protein-bound fraction of donepezil in healthy human plasma, the plasma IC50 of donepezil in the free fraction is estimated to be 9.6 nM.

AChE activity, the relationship between AChE inhibitors and the extent of the central AChE inhibition process has been merely inferred from peripheral measures, such as by red blood cell (RBC) membrane AChE assays. The plasma concentration of donepezil is directly related to RBC AChE inhibition; it is reported to be 63.9% in the 5 mg/day treatment.[1] The RBC AChE inhibition serves as a convenient surrogate marker, per se, but it is not a valid marker for the central AChE inhibition process because inhibition in different tissues is a consequence of specific pharmacokinetics and pharmacodynamics that determine donepezil's accessibility to regional AChE. Currently, no peripheral surrogate marker has a valid one-to-one relationship with regional AChE inhibition in the brain.[12] Therefore, we did not perform RBC AChE assays.

There are several cholinesterase (ChE) inhibitors or the derivatives, such as methyl-tacrine,[28,29] physostigmine,[30] donepezil,[31] CP126 998, and 2-fluoro-CP118 954 labeled with ^{11}C or ^{18}F[32] for measurement of AChE binding sites. Most of them are not selective for AChE and have a considerable amount of non-AChE binding.[33] [^{11}C]donepezil has been applied to measure the effect of donepezil on AChE,[31] but it has high affinity for sigma receptor in addition to the AChE binding site.[34] The kinetic analysis of most radiolabeled ChE inhibitors, such as [^{11}C]donepezil, yields the distribution volume, which is the ratio between the brain concentration and plasma concentration of radioligands at equilibrium state.

In contrast, [^{11}C]MP4A and [^{11}C]MP4P are acetylcholine analogues and highly selective substrates for AChE, although [^{11}C]MP4P is somewhat less selective for AChE than [^{11}C]MP4A. Thus, the kinetic analysis of these radiolabeled acetylcholine analogue substrates allows measurement of AChE activity itself but not of the binding sites. These radiolabeled substrates enter the brain and are metabolized highly selectively by AChE. Carbon-11 labeled metabolites are practically irreversibly trapped in the brain and washed out very slowly, whereas unmetabolized substrates come out as the plasma concentration of radiolabeled substrates decreases. Thus, the kinetics of these radiolabeled substrates can be simplified as irreversible tracers, and the kinetic analysis of these radiolabeled substrates produces the k_3 value, an index of AChE activity. Therefore, the effect of donepezil on AChE may be more accurately measured with [^{11}C]MP4A or [^{11}C]MP4P than with the radiolabeled ChE inhibitors. [^{11}C]MP4A and [^{11}C]MP4P have been shown to be useful for the clinical study of dementias and therapeutic monitoring of the effects of cholinesterase inhibitors with reliable reproducibility. We previously assessed the reproducibility of [^{11}C]MP4A PET technique in five healthy controls and found that cortical k_3 values were nonsignificantly changed by −4 ± 10% in the second PET study without donepezil when compared with the baseline study.[13] Likewise, Kuhl et al[12] showed that PET measures of cerebral k_3 values repeated after 2-month intervals differed only by 6%. The level of precision is suitable for test-retest determination of inhibition effects.

In the present study using [^{11}C]MP4A PET, donepezil reduced k_3 values, an index of AChE activity, in the cortex by 34.6 ± 7.3% ($P < 0.0001$) compared with the baseline activity, confirming our preliminary study, which showed that donepezil reduced AChE activity in the cerebral cortex by 39 ± 5%.[13] Kuhl et al[12] investigated the effects of donepezil on AChE activity using [^{11}C]MP4P (PMP) and PET with arterial blood sampling and showed that cerebral cortical inhibition in 6 patients with AD after 5 and 10 mg of donepezil treatment averaged 26 ± 12% and 27 ± 11%, respectively. Bohnen et al[15] also investigated the effects of donepezil (10 mg/day) on cortical AChE activity using [^{11}C]MP4P and analyzed the data using the shape analysis without the plasma input function. The results showed that the average cortical (temporal, parietal, and dorsolateral prefrontal) donepezil-induced AChE inhibition after 10 mg of donepezil treatment in 14 patients with AD was 19.1 ± 9.4% compared with the baseline activity. Because donepezil is a highly selective inhibitor of AChE but not an inhibitor of butyrylcholinesterase, the lower inhibition rates by donepezil in these studies with [^{11}C]MP4P PET could be attributed to lower selectivity of MP4P for AChE than that of MP4A for AChE. The selectivity of MP4A and MP4P for AChE in human cerebral cortex was estimated to be 94% and 86%, respectively, in a postmortem brain study.[35]

Using [^{11}C]MP4A PET, Kaasinen et al[14] performed a study on 6 patients with AD and reported the regional difference in the inhibition rates in the cerebral cortex induced by donepezil. The treatment with 10 mg of donepezil reduced the AChE activity in the AD brain by 39% in the frontal cortex, 29% in the temporal cortex, and 28% in the parietal cortex. The degree of AChE inhibition was significantly greater in the frontal cortex than in the parietal and temporal cortices. Kaasinen et al[14] attributed the regional difference in AChE inhibition to the more severe reduction of AChE activity in the temporal cortex than in the frontal cortex at baseline in patients with AD. This study as well as the study of Kuhl et al[12] showed that the inhibitory effect of donepezil on AChE activity was uniform across the cerebral cortex.

According to the 24-week measurements of RBC AChE inhibition in the 5-mg/day donepezil treatment, the pharmacodynamics of donepezil was stable after 6 weeks of treatment.[36] The elimination of donepezil from the plasma was relatively slow at the 4.0- and 6.0-mg dose levels with an apparent half-life of approximately 80 hours.[25] The steady-state plasma concentration of donepezil after oral doses of 5 mg/day was reported as 29.6 ng/mL after 12 weeks of treatment in patients with AD[1] and 26.4 ± 3.9 ng/ml after 28 days of administration in healthy subjects.[37] The plasma concentration of donepezil in patients with AD in the present study (28.9 ng/mL) was almost the same in these previous studies.

To the best of our knowledge, there has been no in vivo human study concerning the quantitative relationship between

the plasma donepezil concentration and brain AChE inhibition. Readers may notice that data point in Figure 1 only cover narrow range of the total curve, and the correlation coefficient between the plasma donepezil concentration and the AChE inhibition rate remained 0.50 (borderline significantly higher correlation). The insufficient correlation rate may be due to the restricted regimen. At the time of this study, the dosing regimen in Japan was strictly set at daily doses of 3 mg for 2 weeks, followed by 5 mg/day, whereas taking 10 mg daily was not approved for clinical use, although it is available now. A wider range of donepezil doses would have revealed a significant correlation between the plasma donepezil concentration and the AChE inhibition rate. Indeed in vitro human study[19] and in vivo monkey study[17] showed that the inhibitory effects of AChE inhibitors are dose dependent on AChE activity. This premise encouraged us to estimate the in vivo plasma IC_{50} of donepezil for brain AChE inhibition in patients with AD. Currently, no peripheral surrogate marker, such as RBC AChE, has a valid one-to-one relationship with regional AChE inhibition in the brain.[12] Once the in vivo plasma IC_{50} of donepezil is estimated, the AChE inhibition rates in the cerebral cortex can be determined from the plasma concentration of donepezil in each patient with AD at various doses subsequently. Therefore, the in vivo plasma IC_{50} of donepezil is worthy to be estimated despite of the high costs and efforts for PET studies.

The plasma IC_{50} value was estimated at 54 ng/mL (130 nM) in the present study. Using the reported protein-bound fraction (92.6%) of donepezil in healthy human plasma,[38] we could estimate the plasma IC_{50} of donepezil in the free fraction as 9.6 nM (130 nM × [100-92.6]%). Both Yamanishi et al[39] and Ogura et al,[40] using rat brain homogenate at a highly diluted condition where protein binding is considered to be negligible, reported in vitro IC_{50} of donepezil as 6.7 nM. We previously estimated in vivo plasma IC_{50} of donepezil to be 6.6 nM in free fraction in 5 rhesus monkeys using [^{11}C]MP4A PET.[17] The slight difference in plasma IC_{50} of donepezil between these animal studies and the present human study could be attributed to the methodological differences in addition to species differences.

In summary, we estimated the in vivo plasma IC_{50} of donepezil for brain AChE inhibition in patients with AD to be 54 ng/mL (130 nM). Once the plasma IC_{50} of donepezil is determined, the brain AChE inhibition rate could be estimated from the plasma concentration of donepezil in each subject based on the plasma IC_{50}. Subsequently, the AChE inhibition rates in the cerebral cortex can be estimated from the plasma concentration of donepezil in each patient with AD at various doses. Now that the mean donepezil concentrations in the plasma at the dose of 5 mg/day remained 28.9 ng/mL, approximately half of the plasma IC_{50}, higher dose of donepezil might provide further benefits for patients with AD, if safe and tolerated. This technique can be also applied to measure the in vivo plasma IC_{50} of other ChE inhibitors, such as rivastigmine and galantamine, and may facilitate the determination of appropriate clinical dosages of cholinesterase inhibitors.

ACKNOWLEDGMENT

The authors thank the staff of the Department of Medical Imaging, National Institute of Radiological Sciences for supplying [^{11}C]MP4A and providing technical support for PET data acquisition.

REFERENCES

1. Rogers SL, Friedhoff LT, the Donepezil Study Group. The efficacy and safety of donepezil in patients with AD: results of a US multicentre, randomized, double-blind, placebo-controlled trial. *Dementia* 1996;7:293–303.
2. Kimura M, Asasofu S, Ogura H, et al. Protective effect of donepezil against Abeta (1–40) neurotoxicity in rat septal neurons. *Brain Res* 2005;14:72–84.
3. Ballard CG, Chalmers KA, Todd C, et al. Cholinesterase inhibitors reduce cortical Abeta in dementia with Lewy bodies. *Neurology* 2007;68:1726–1729.
4. Van Dam D, Coen K, De Deyn PP. Cognitive evaluation of disease-modifying efficacy of donepezil in the APP 23 mouse model for Alzheimer's disease. *Psychopharmacology (Berl)* 2008;197:37–43.
5. Irie T, Fukushi K, Akimoto Y, et al. Design and evaluation of radioactive acetylcholine analogues for mapping brain acetylcholinesterase (AChE) *in vivo*. *Nucl Med Biol* 1994;21:801–808.
6. Kilbourn MR, Snyder SE, Sherman PS, et al. *In vivo* studies of acetylcholinesterase activity using a labeled substrate, *N*-[^{11}C]methylpiperidin-4-*yl* propionate ([^{11}C]PMP). *Synapse* 1996;22:123–131.
7. Namba H, Iyo M, Fukushi K, et al. Human cerebral acetylcholinesterase activity measured with positron emission tomography: procedure, normal value and effect of age. *Eur J Nucl Med* 1999;26:135–143.
8. Koeppe RA, Frey KA, Snyder SE, et al. Kinetic modeling of *N*-[^{11}C]methylpiperidin-4-*yl* propionate: alternatives for analysis of an irreversible positron emission tomography tracer for measurement of acetylcholinesterase activity in human brain. *J Cereb Blood Flow Metab* 1999;19:1150–1163.
9. Iyo M, Namba H, Fukushi K, et al. Measurement of acetylcholinesterase by positron emission tomography in the brains of healthy controls and patients with Alzheimer's disease. *Lancet* 1997;349:1805–1809.
10. Kuhl DE, Koeppe RA, Minoshima S, et al. In vivo mapping of cerebral acetylcholinesterase activity in aging and Alzheimer's disease. *Neurology* 1999;52:691–699.
11. Shinotoh H, Namba H, Yamaguchi M, et al. Positron emission tomographic measurement of acetylcholinesterase activity reveals differential loss of ascending cholinergic systems in Parkinson's disease and progressive supranuclear palsy. *Ann Neurol* 1999;46:62–69.
12. Kuhl DE, Minoshima S, Frey KA, et al. Limited donepezil inhibition of acetylcholinesterase measured with positron emission tomography in living Alzheimer's cerebral cortex. *Ann Neurol* 2000;48:391–395.
13. Shinotoh H, Aotsuka A, Fukushi K, et al. Effect of donepezil on brain acetylcholinesterase activity in patients with AD measured by PET. *Neurology* 2001;56:408–410.
14. Kaasinen V, Någren K, Järvenpää T, et al. Regional effects of donepezil and rivastigmine on cortical acetylcholinesterase activity in Alzheimer's disease. *J Clin Psychopharmacol* 2002;22:615–620.
15. Bohnen NI, Kaufer DI, Hendrickson R, et al. Degree of inhibition of acetylcholinesterase activity and cognitive effects by donepezil treatment in Alzheimer's disease. *J Neurol Neurosurg Psychiatry* 2005;76:315–319.
16. Tsukada H, Nishiyama S, Fukumoto D, et al. Effects of acute acetylcholinesterase inhibition on the cerebral cholinergic neuronal system and cognitive function: functional imaging of the conscious monkey brain using animal PET in combination with microdialysis. *Synapse* 2004;52:1–10.
17. Shiraishi T, Kikuchi T, Fukushi K, et al. Estimation of plasma IC50 of donepezil hydrochloride for brain acetylcholinesterase inhibition in monkey using *N*-[11C]methylpiperidin-4-*yl* acetate ([^{11}C]MP4A) and PET. *Neuropsychopharmacology* 2005;30:2154–2161.
18. Kadir A, Darreh-Shori T, Almkvist O, et al. PET imaging of the in vivo brain acetylcholinesterase activity and nicotine binding in galantamine-treated patient with AD. *Neurobiol Aging* 2008;29:1204–1217.
19. Kasa P, Papp H, Kasa P Jr, et al. Donepezil dose-dependently inhibits

acetylcholinesterase activity in various areas and in the presynaptic cholinergic and the postsynaptic cholinoceptive enzyme-positive structures in human and rat brain. *Neuroscience* 2000;101:89–100.

20. McKhann G, Drachman D, Folstein M, et al. Clinical diagnosis of Alzheimer's disease: report of the NINCDS-ADRDA Work Group under the auspices of Department of Health and Human Services Task Force on Alzheimer's disease. *Neurology* 1984;34:939–944.
21. Namba H, Tanaka N, Matsuura H, et al. Pixel-by-pixel mapping of acetylcholinesterase activity in human brain with [^{11}C]MP4A/PET. In: Senda M, Kimura Y, Herscovitch P, ed. *Brain Imaging Using PET.* 1st ed. San Diego, CA: Academic Press; 2002:55–61.
22. Mizumura S, Kumita S, Cho K, et al. Development of quantitative analysis method for stereotactic brain image: assessment of reduced accumulation in extent and severity using anatomical segmentation. *Ann Nucl Med* 2003;17:289–295.
23. Lancaster JL, Woldorff MG, Parsons LM, et al. Automated Talairach Atlas labels for functional brain mapping. *Hum Brain Mapp* 2000;10:120–131.
24. Lee JW, Rogers SL, Friedhoff LT, et al. Validation and application of an HPLC method for the determination on 1-benzyl-4-[(5,6-dimethoxy-1-indanon)-2-*yl*] methyl piperidine HCl (E2020) in human plasma. *Pharm Res* 1992;9:S338.
25. Rogers SL, Friedhoff LT. Pharmacokinetic and pharmacodynamic profile of donepezil HCl following single oral doses. *Br J Clin Pharmacol* 1998a;46(suppl 1):1–6.
26. Carson RE. Parameter estimation in positron emission tomography. In: Phelps M, Mazziotta J, Schelbert H, ed. *Positron Emission Tomography and Autoradiography: Principles and Applications for the Brain and Heart.* New York: Raven Press; 1986:347–390.
27. Veng PP. Curve fitting and modeling in pharmacokinetics and some practical experiences with NONLIN and a new program FUNFIT. *J Pharmacokinet Biopharm* 1977;5:513–531.
28. Bonnot-Lours S, Prenant C, Crouzel C. Synthesis of 9-[^{11}C]methylamino-1,2,3,4-tetrahydroacridine, a potent acetylcholinesterase inhibitor. *Appl Radiat Isot* 1991;41:690–691.
29. Traykov L, Tavitian B, Jobert A, et al. In vivo PET study of cerebral [^{11}C]methyl-tetrahydroaminoacridine distribution and kinetics in healthy human subjects. *Eur J Neurol* 1999;6:273–278.
30. Pappata S, Tavitian B, Traykov L, et al. In vivo imaging of human cerebral acetylcholinesterase. *J Neurochem* 1996;67:876–879.
31. Okamura N, Funaki Y, Tashiro M, et al. In vivo visualization of donepezil binding in the brain of patients with Alzheimer's disease. *Br J Clin Pharmacol* 2008;65:472–479.
32. Musachio JL, Flesher JE, Scheffel UA, et al. Radiosynthesis and mouse brain distribution studies of [^{11}C]CP-126,998: a PET ligand for in vivo study of acetylcholinesterase. *Nucl Med and Biol* 2002;29: 547–552.
33. Kikuchi T, Okamura T, Fukushi K, et al. Cerebral acetylcholinesterase imaging: development of the radioprobes. *Curr Top Med Chem* 2007;18:1790–1799.
34. Kato K, Hayako H, Ishihara Y, et al. TAK-147, an acetylcholinesterase inhibitor, increases choline acetyltransferase activity in cultured rat septal cholinergic neurons. *Neurosci Lett* 1999;260:5–8.
35. Irie T, Fukushi K, Namba H, et al. Brain acetylcholinesterase activity: validation of a PET tracer in a rat model of Alzheimer's disease. *J Nucl Med* 1996;37:649–655.
36. Rogers SL, Farlow MR, Doody RS, et al. A 24-week, double-blind, placebo-controlled trial of donepezil in patients with Alzheimer's disease. *Neurology* 1998b;50:136–145.
37. Tiseo PJ, Rogers SL, Friedhoff LT. Pharmacokinetic and pharmacodynamic profile of donepezil HCl following evening administration. *Br J Clin Pharmacol* 1998;46(suppl 1):13–18.
38. Mihara M, Ohnishi A, Tomono Y, et al. Pharmacokinetics of E2020, a new compound for Alzheimer's disease, in healthy male volunteers. *Int J Clin Pharmacol Ther Toxicol* 1993;31:223–229.
39. Yamanishi Y, Kosasa T, Kuriya Y. Inhibitory effect of donepezil hydrochloride on cholinesterase activities in vitro. *Jpn Pharmacol Ther* 1998;26(suppl):1277–1282 (in Japanese).
40. Ogura H, Kosasa T, Kuriya Y, et al. Comparison of inhibitory activities of donepezil and other cholinesterase inhibitors on acetylcholinesterase and butyrylcholinesterase in vitro. *Methods Find Exp Clin Pharmacol* 2000;22:609–613.

Eur J Nucl Med Mol Imaging
DOI 10.1007/s00259-009-1314-7

ORIGINAL ARTICLE

In vivo detection of prion amyloid plaques using [^{11}C]BF-227 PET

Nobuyuki Okamura · Yusei Shiga · Shozo Furumoto · Manabu Tashiro · Yoshio Tsuboi · Katsutoshi Furukawa · Kazuhiko Yanai · Ren Iwata · Hiroyuki Arai · Yukitsuka Kudo · Yasuhito Itoyama · Katsumi Doh-ura

Received: 7 August 2009 / Accepted: 21 October 2009

Abstract
Purpose In vivo detection of pathological prion protein (PrP) in the brain is potentially useful for the diagnosis of transmissible spongiform encephalopathies (TSEs). However, there are no non-invasive ante-mortem means for detection of pathological PrP deposition in the brain. The purpose of this study is to evaluate the amyloid imaging tracer BF-227 with positron emission tomography (PET) for the non-invasive detection of PrP amyloid in the brain.
Methods The binding ability of BF-227 to PrP amyloid was investigated using autoradiography and fluorescence microscopy. Five patients with TSEs, including three patients with Gerstmann-Sträussler-Scheinker disease (GSS) and two patients with sporadic Creutzfeldt-Jakob disease (CJD), underwent [^{11}C]BF-227 PET scans. Results were compared with data from 10 normal controls and 17 patients with Alzheimer's disease (AD). The regional to pons standardized uptake value ratio was calculated as an index of BF-227 retention.
Results Binding of BF-227 to PrP plaques was confirmed using brain samples from autopsy-confirmed GSS cases. In clinical PET study, significantly higher retention of BF-227 was detected in the cerebellum, thalamus and lateral temporal cortex of GSS patients compared to that in the corresponding tissues of normal controls. GSS patients also showed higher retention of BF-227 in the cerebellum, thalamus and medial temporal cortex compared to AD patients. In contrast, the two CJD patients showed no obvious retention of BF-227 in the brain.
Conclusion Although [^{11}C]BF-227 is a non-specific imaging marker of cerebral amyloidosis, it is useful for in vivo detection of PrP plaques in the human brain in GSS, based on the regional distribution of the tracer. PET amyloid imaging might provide a means for both early diagnosis and non-invasive disease monitoring of certain forms of TSEs.

N. Okamura · S. Furumoto · K. Yanai
Department of Pharmacology,
Tohoku University School of Medicine,
Sendai, Japan

Y. Shiga · Y. Itoyama
Department of Neurology,
Tohoku University School of Medicine,
Sendai, Japan

S. Furumoto · R. Iwata
Division of Radiopharmaceutical Chemistry,
Cyclotron and Radioisotope Center, Tohoku University,
Sendai, Japan

M. Tashiro
Division of Cyclotron Nuclear Medicine,
Cyclotron and Radioisotope Center, Tohoku University,
Sendai, Japan

Y. Tsuboi
Department of Neurology,
Fukuoka University School of Medicine,
Fukuoka, Japan

K. Furukawa · H. Arai
Department of Geriatrics and Gerontology,
Division of Brain Sciences, Institute of Development,
Aging, and Cancer, Tohoku University,
Sendai, Japan

Y. Kudo
Innovation of New Biomedical Engineering Center,
Tohoku University,
Sendai, Japan

K. Doh-ura (✉)
Department of Prion Research,
Tohoku University School of Medicine,
2-1 Seiryo-machi, Aoba-ku, Sendai 980-8575, Japan
e-mail: doh-ura@mail.tains.tohoku.ac.jp

Published online: 17 December 2009

Keywords Prion · PET · Amyloid · Creutzfeldt-Jakob disease

Introduction

Transmissible spongiform encephalopathies (TSEs), also known as prion diseases, are a group of fatal neurodegenerative disorders, including Creutzfeldt-Jakob disease (CJD), Gerstmann-Sträussler-Scheinker disease (GSS) and kuru [1–3]. TSEs are characterized by progressive deposition of abnormal prion protein (PrP) in the brain. CJD is the most common type of human TSE and is classified into sporadic, genetic and infectious forms according to the aetiology of illness. GSS is a familial neurodegenerative disorder associated with mutations of the PrP gene and is clinically recognized by cerebellar ataxia combined with postural abnormalities and cognitive decline [1–3]. Two major types of abnormal PrP deposition, synaptic and plaque types, have been described in the brain of people with TSEs [1]. The synaptic type of PrP deposition, which does not have tinctorial properties of amyloid in tissue sections, is most commonly observed in sporadic CJD, whereas the plaque type, which frequently forms congophilic amyloid plaques, is a hallmark of such TSEs as GSS, variant CJD (vCJD) and iatrogenic dura CJD with plaques [1, 4]. Abnormal PrP deposition in the brain is suggested to start before the occurrence of clinical symptoms [5–7]. Thus, preclinical diagnosis and, when available, early disease-specific therapeutic interventions, can be beneficial for people predisposed to or affected by TSEs.

Several positron emission tomography (PET) imaging agents have been recently developed and used for in vivo detection of brain amyloid-β (Aβ) plaques in patients with Alzheimer's disease (AD) [8–12]. Most of these β-sheet binding agents show high binding affinity to PrP amyloid because PrP aggregates in TSEs form β-pleated sheet structures and share a common secondary structure with Aβ deposits in AD brains [13–16]. Therefore, these agents would be useful for the in vivo detection of PrP amyloid in the brain. Two clinical PET studies were performed using [^{18}F]FDDNP and/or [^{11}C]PIB in sporadic and familial CJD patients [17, 18]. The results indicated moderate retention of FDDNP and no obvious retention of PIB in the brain [17, 18]. Therefore, agents that can sensitively detect abnormal PrP deposits should be further explored for the diagnosis of TSEs. We have demonstrated in vitro and in vivo binding of benzoxazole derivatives to both Aβ and PrP amyloids [19, 20]. One of these derivatives, BF-227, was used for a clinical PET study where it successfully visualized amyloid deposits in the brain of AD patients in vivo [12, 21]. Therefore, [^{11}C]BF-227 appears to be a promising candidate for PET imaging of PrP deposits. The purpose of this study was to evaluate the clinical utility of [^{11}C]BF-227 PET for the non-invasive detection of abnormal PrP deposits in patients with TSEs.

Methods

Preparation of compounds

BF-227 and its 2-tosyloxyethoxy and *N*-desmethylated derivatives were custom synthesized by Tanabe R&D Service Co. (Osaka, Japan). [^{18}F]BF-227 was synthesized for autoradiography of brain sections, as described previously [22]. For the clinical studies, [^{11}C]BF-227 was synthesized as described previously [12]. Radiochemical yields were greater than 50% based on [^{11}C]methyl triflate, and specific radioactivities were 119–138 GBq/μmol at the end of synthesis. Radiochemical purities were greater than 95%.

Histopathological staining and in vitro autoradiography

Autopsy-diagnosed brain samples from two GSS cases with PrP plaque deposition and two sporadic CJD cases with synaptic PrP deposition were provided by Dr. Toru Iwaki of the Department of Neuropathology, Kyushu University, Japan. The brain sample from an 81-year-old man with autopsy-confirmed physiological aging was obtained from Tohoku University Hospital. The two GSS cases had a proline-to-leucine mutation at codon 102 and methionine homozygosity at codon 129 of the PrP gene, and the two sporadic CJD cases had no mutations and methionine homozygosity at codon 129; they showed type 1 abnormal PrP in immunoblotting of the brain tissues. All of the brain samples were treated with 98% formic acid for 1 h before paraffin embedding to eliminate prion infectivity. Sections from paraffin-embedded blocks of the cerebellum or frontal cortex were then dewaxed in xylene and ethanol. For staining with BF-227, tissue sections were immersed in 100 μM BF-227 solution containing 50% ethanol for 10 min. They were then dipped briefly into water and rinsed in phosphate-buffered saline for 10 min before coverslipping with FluorSave Reagent (Calbiochem, La Jolla, CA, USA). Subsequently, they were examined using an Eclipse E800 microscope (Nikon, Tokyo, Japan) equipped with a V-2A filter set (excitation, 380–420 nm; dichroic mirror, 430 nm; Longpass filter, 450 nm). For autoradiography, the section was incubated with 1.0 MBq/ml of [^{18}F]BF-227 at room temperature for 10 min and then washed briefly with water and 50% ethanol. After drying, the labelled section was exposed to a BAS-III imaging plate (Fuji Film, Tokyo, Japan) overnight. Autoradiographic images were obtained using a BAS-5000 phosphor imaging instrument (Fuji Film, Tokyo, Japan). Neighbouring sec-

tions were immunostained using 3F4 anti-PrP monoclonal antibody (Covance, Princeton, NJ, USA) as described previously [13, 20].

Subjects and patients in the clinical PET study

Five TSE patients, including two sporadic CJD patients [63-year-old woman (CJD1) and 58-year-old man (CJD2)] and three GSS patients [69-year-old woman (GSS1), 61-year-old man (GSS2) and 30-year-old woman (GSS3)], underwent PET scans with [^{11}C]BF-227 (Table 1). For comparison, [^{11}C]BF-227 PET studies were also performed in 17 AD patients [mean age ± standard deviation (SD)= 72.6±6.7; mean Mini-Mental State Examination score ± SD=19.8±4.0] and 10 aged normal controls (mean age ± SD=67.2±2.5). Some of these AD and normal subjects were included in our previous report [12].

CJD1's health was unremarkable until the manifestation of depressive symptoms at the age of 62 years. The patient then developed subacutely progressive dementia, motor disturbances and myoclonus. CJD2 showed subacutely progressive dementia and gait disturbance and then developed psychotic symptoms, dysarthria and myoclonus. Both CJD patients had no mutations and showed methionine homozygosity at codon 129 of the PrP gene. PET studies in CJD1 and CJD2 were performed when they reached grade 4 of the modified Rankin scale at 3 and 4 months after onset of symptoms, respectively. Both patients showed periodic synchronous discharges in electroencephalograms and hyperintensity in the caudate, putamen and cerebral cortex on diffusion-weighted magnetic resonance (MR) images. Diagnosis of probable CJD was made according to the WHO criteria [23].

Each GSS patient was from a different pedigree and had a family history of the same disease, carrying a proline-to-leucine mutation at codon 102 and methionine homozygosity at codon 129 of the PrP gene. GSS1 and GSS2, having a 9- and 20-month clinical duration from the onset, respectively, showed signs of moderate cerebellar ataxia, such as gait disturbance and slurred speech; however, they could walk unassisted and had slight or no cognitive impairment. GSS1 and GSS2 scored 22 and 26 points, respectively, on the Mini-Mental State Examination. GSS3, having a 27-month clinical duration, showed severe gait disturbance and slurred speech and was unable to walk unassisted; however, she had no cognitive impairment (30 points on the Mini-Mental State Examination) at the time of this study.

AD diagnosis was made according to the National Institute of Neurological and Communicative Diseases and Stroke-Alzheimer's Disease and Related Disorders Association (NINCDS-ADRDA) criteria [24]. CJD, GSS and AD patients were recruited from Miyagi National Hospital, Fukuoka University Hospital, Kagoshima University Hospital and Tohoku University Hospital. Normal controls were recruited from volunteers with no cognitive impairment or cerebrovascular lesions on MR images and who were not taking any centrally acting medications. No significant difference in age distribution was apparent between the groups. This study was approved by the Ethics Committee on clinical investigations of Tohoku University School of Medicine and performed in accordance with the Declaration of Helsinki. Written informed consent was obtained after complete description of the study to the patients and subjects.

Image acquisition protocols

PET scans were performed using a SET-2400W (Shimadzu Inc., Kyoto, Japan). After intravenous injection of 211–366 MBq (5.7–9.9 mCi) of [^{11}C]BF-227, dynamic PET images were obtained for 60 min with the subjects' eyes closed. Arterial blood sampling in the TSE patients was not

Table 1 Regional to pons standardized uptake value ratio (SUVRp) values in aged normal controls (Control), Alzheimer's disease patients (AD), Creutzfeldt-Jakob disease patients (CJD) and Gerstmann-Sträussler-Scheinker disease patients (GSS)

	Control (n=10) Mean ± SD	AD (n=17) Mean ± SD	CJD1	CJD2	GSS (n=3) Mean ± SD	GSS1	GSS2	GSS3
Frontal	0.60±0.03	0.64±0.04	0.57	0.61	0.67±0.08	0.74	0.69	0.57
Lateral temporal	0.59±0.03	0.69±0.04*	0.63	0.62	0.67±0.05*	0.71	0.68	0.61
Parietal	0.62±0.02	0.69±0.04*	0.62	0.62	0.67±0.06	0.72	0.68	0.61
Occipital	0.62±0.04	0.65±0.05	0.62	0.69	0.67±0.07	0.74	0.67	0.60
Medial temporal	0.64±0.04	0.62±0.03	0.57	0.65	0.67±0.02**	0.66	0.70	0.67
Striatum	0.71±0.04	0.75±0.04*	0.69	0.72	0.76±0.04	0.80	0.77	0.72
Thalamus	1.00±0.04	1.01±0.04	0.97	1.04	1.08±0.00*, **	1.08	1.07	1.08
Cerebellum	0.58±0.01	0.57±0.02	0.58	0.59	0.62±0.01*, **	0.61	0.63	0.61

*p<0.05 compared to aged normal group

**p < 0.05 compared to AD group

performed because the Committee on Clinical Investigation at Tohoku University School of Medicine did not approve blood sampling during the PET scan, from the standpoint of infection risk management. T_1-weighted MR images were obtained using a Signa 1.5-T machine (General Electric Inc., Milwaukee, WI, USA).

Image analysis

Standardized uptake value (SUV) images of [^{11}C]BF-227 were obtained by normalizing tissue concentration by injected dose and body weight. Average summations of SUV images were created from early frames (0–30 min post-injection) and late frames (40–60 min post-injection) of dynamic PET images. Early frame images were created for co-registration with individual MR images, and late frame images were used for calculation of SUV. Individual MR images were anatomically co-registered with the early frame PET images using statistical parametric mapping software (SPM2, Welcome Department of Imaging Neuroscience, London, UK) [25]. Spatial normalization was performed using an MR T_1 template of SPM2 to transfer PET images into a standard stereotactic space. Regions of interest (ROIs) were placed on a spatially normalized MR image, as described previously [12]. ROI information was then copied onto delayed PET SUV images, and regional SUV images at 40–60 min post-injection were sampled using Dr.View/LINUX software (AJS, Tokyo, Japan). Deposition of PrP plaques is reportedly frequent in the cerebellum but scarce in the pons of GSS brain [26]. Furthermore, BF-227 retention in the pons does not differ between AD patients and normal controls. Therefore, we used the pons as a reference region and calculated the regional to pons SUV ratio (SUVRp) as an index of BF-227 retention.

Statistical analysis

For statistical comparison in each group, we applied one-way analysis of variance, followed by the Bonferroni-Dunn post hoc test. Statistical comparison of age distribution was performed using the Kruskal-Wallis test, followed by Dunn's multiple comparison test. Statistical significance for each analysis was defined as $p<0.05$.

Results

Autoradiography examination indicated binding of a tracer dose of BF-227 to PrP plaque deposits. BF-227 retention was present in brain sections from GSS cases with PrP plaque deposition but not from normal control cases and sporadic CJD cases with synaptic PrP deposition (Fig. 1a–c). The regional distribution of [^{18}F]BF-227 in the autoradiograms co-localized with the immunostained PrP plaques in the cerebellar cortex of GSS cases (Fig. 1d–e). BF-227 binding to PrP plaques was additionally examined using a microscope, because BF-227 is a fluorescent compound. Core regions of the PrP plaques were intensely stained with BF-227 (Fig. 2, arrows), indicating that BF-227 preferentially binds to the fibril-rich core of PrP amyloid plaques.

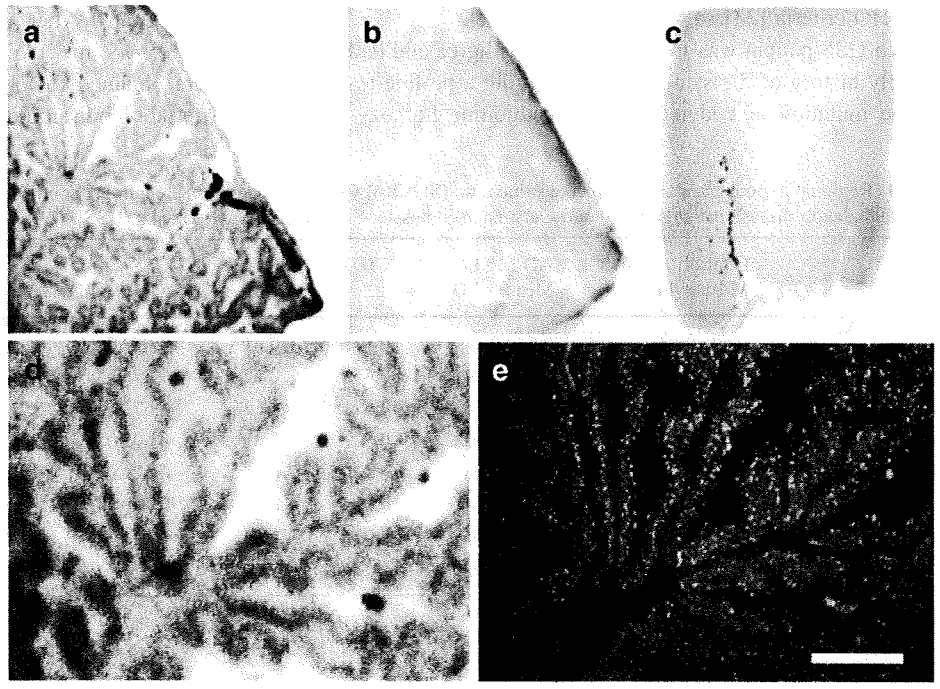

Fig. 1 [^{18}F]BF-227 autoradiograms of a cerebellar section from a Gerstmann-Sträussler-Scheinker (GSS) case (**a**), a cerebellar section from a physiological aging case (**b**) and a frontal cortex section from a sporadic Creutzfeldt-Jakob disease (CJD) case (**c**) are shown, together with a magnified view of **a** (**d**) and prion protein (PrP) immunostaining of the same field as **d** (**e**). BF-227 retention was present in the brain section from a GSS case with PrP plaque deposition, but not from a normal control case and sporadic CJD case with synaptic PrP deposition. *Bar*=200 μm

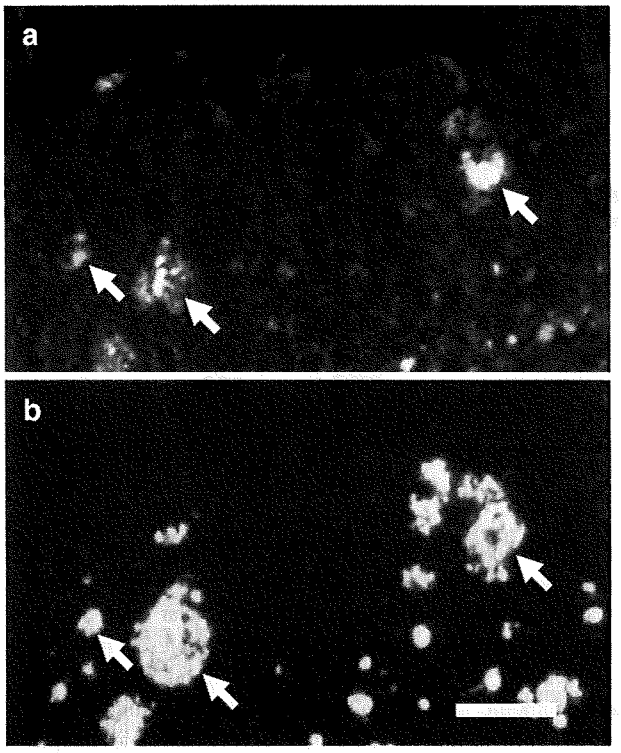

Fig. 2 Microscopic images of BF-227 staining (**a**) and PrP immunostaining (**b**) of the cerebellar cortex of a GSS case. *Arrows* indicate PrP amyloid plaques. The core regions of PrP plaques were intensely stained with BF-227. *Bar*=50 μm

Figure 3 shows the average summations of SUVRp images in an aged normal subject (64-year-old man), a sporadic CJD patient (CJD1, 63-year-old woman), a GSS patient (GSS2, 61-year-old man) and an AD patient (62-year-old woman). As reported previously, non-specific retention of [^{11}C]BF-227 was observed in the brain stem and white matter of all subjects [12]. The GSS patient showed obvious retention of [^{11}C]BF-227 in the cerebellum, and lateral and medial temporal cortices. The three GSS patients showed significantly higher SUVRp in the lateral temporal cortex, thalamus and cerebellum (Table 1, Fig. 4) when compared to aged normal controls. Furthermore, when compared to the AD group, the GSS group showed significant elevation of SUVRp in the medial temporal cortex, thalamus and cerebellum. Although two GSS patients (GSS1 and GSS2) showed retention of BF-227 in most brain regions, the youngest GSS patient (GSS3) showed BF-227 retention only in the cerebellum, thalamus and medial temporal cortex, but not in the neocortex (Table 1, Fig. 4). Furthermore, two sporadic CJD patients showed no obvious BF-227 retention in any of the brain regions examined (Table 1, Fig. 4). As previously described [12, 21], AD patients showed [^{11}C]BF-227 retention in the neocortex; however, the cerebellum and medial temporal cortex were relatively spared (Table 1).

Autopsy examination of the brain of one GSS patient (GSS1) confirmed both the presence of abundant PrP amyloid plaques in the neocortex, cerebellum, basal ganglia, thalamus, entorhinal cortex and hippocampus and the absence of Aβ amyloid plaques or other structures of misfolded protein deposition such as Lewy bodies and neurofibrillary tangles. When compared to controls, the highest SUVRp percentage difference was found in the neocortex, especially in the frontal cortex (22%), followed by the striatum (12%), thalamus (9%), cerebellum (6%) and medial temporal cortex (3%) in this case. This finding was consistent with the autopsy result showing higher density of PrP amyloid plaques in the neocortex and basal ganglia than in the cerebellum, thalamus and hippocampus. Details of clinicopathological features of this case will be published elsewhere.

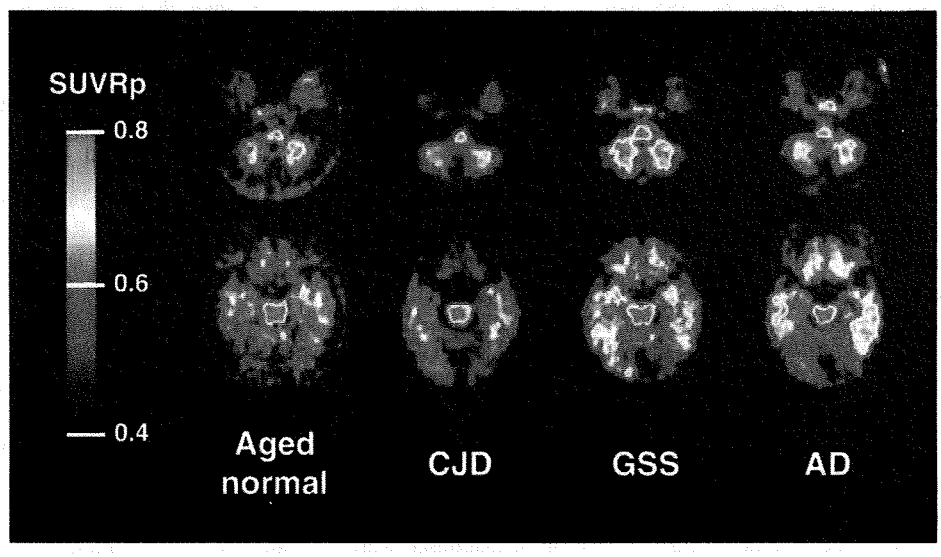

Fig. 3 Mean regional to pons standardized uptake value ratio (SUVRp) images between 40 and 60 min post-injection of [^{11}C]BF-227 in an aged normal subject (64-year-old man), a sporadic CJD patient (CJD1, 63-year-old woman), a GSS patient (GSS2, 61-year-old man) and an AD patient (62-year-old woman). Compared to the aged normal subject and CJD patient, the GSS patient showed obvious [^{11}C]BF-227 retention in the cerebellum and temporal cortex. The AD patient also showed obvious [^{11}C]BF-227 retention in the temporal cortex; however, the cerebellum was relatively spared

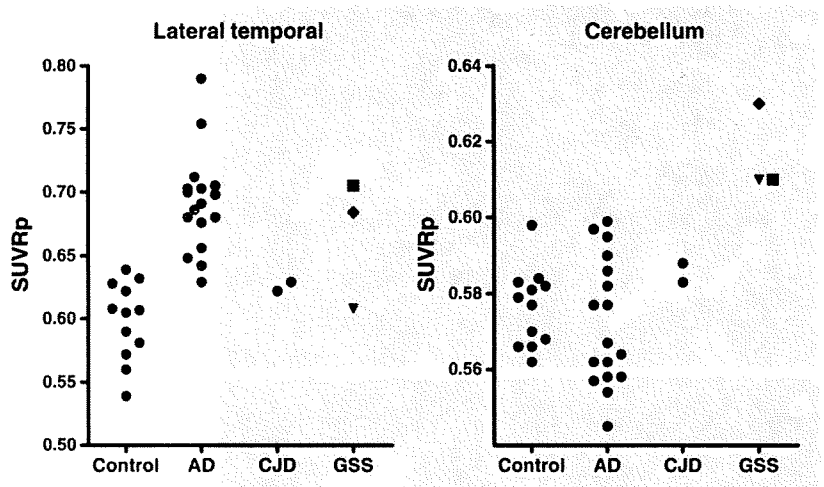

Fig. 4 SUVRp distribution in aged normal controls (*Control*), AD patients (*AD*), CJD patients (*CJD*) and GSS patients (*GSS*). GSS patients showed higher SUVRp values in the lateral temporal cortex and cerebellum. *Filled square* GSS1, *filled diamond* GSS2, *filled inverted triangle* GSS3

Discussion

This is the first study to demonstrate non-invasive detection of PrP amyloid plaques in GSS patients. GSS is neuropathologically characterized by deposits of multicentric amyloid plaques, which are especially abundant in the cerebellum, cerebral cortex and basal ganglia [3]. The present study demonstrated binding of BF-227 to PrP amyloid plaques in GSS brain sections. [^{11}C]BF-227 retention was observed in cortical and subcortical brain regions of GSS patients known for the high density of PrP plaques. Based on these findings, [^{11}C]BF-227 represents a promising candidate PET probe for the non-invasive detection of PrP amyloid plaques in the brain. However, the possibility that neocortical elevation of SUVRp in GSS patients might be caused by concomitant Aβ amyloid deposits or other misfolded protein deposits also should be considered, given that the two GSS patients showing prominent neocortical retention of [^{11}C]BF-227 were relatively older than the GSS patient showing no neocortical retention of BF-227. Although one positive GSS patient (GSS2) is still alive and was not examined neuropathologically, another positive case (GSS1) showed a high level of PrP amyloid deposits but no obvious deposits of Aβ amyloid or other misfolded proteins at autopsy. Furthermore, significant elevation of SUVRp was detected in the cerebellum, thalamus and hippocampus of all GSS cases. These brain regions are known to contain lower densities of Aβ plaques or other misfolded protein structures such as Lewy bodies. Based on these findings, it seems unlikely that concomitant deposition of Aβ amyloid or other misfolded proteins contributes to the high [^{11}C]BF-227 retention in GSS patients.

There is an increasing demand for in vivo detection of abnormal PrP deposition in the brain for the diagnosis of TSEs that might translate in early therapeutic intervention. Although GSS and other familial forms of TSEs can be diagnosed with PrP gene analysis using peripheral blood cells, it has been impossible to non-invasively measure the amount of abnormal PrP deposition in the brain. In a fashion similar to GSS, PrP amyloid deposition in the brain is commonly present in vCJD in which PrP amyloid plaques, called florid plaques, are pathognomonic [27]. Thus, [^{11}C]BF-227 PET might be a sensitive probe for the detection of PrP amyloid plaque deposition in vCJD as well as GSS, allowing longitudinal monitoring of PrP amyloid plaque deposition in the brain. Ante-mortem diagnosis of vCJD relies on the detection of abnormal PrP deposition in tonsil biopsy samples [28]. However, functional imaging using PET has an advantage over surgical biopsy tests in terms of both a non-invasive and an infection risk management point of view.

GSS is a rare form of TSE occurring in only about 3% of TSE cases in Japan. However, GSS is probably one of the TSEs most likely to benefit from early therapeutic interventions because the disease can be confirmed earlier using PrP gene analysis and progression occurs much more slowly than that in sporadic CJD, which comprises the majority of TSE cases. Recently, compounds such as pentosan polysulphate and doxycycline have been clinically used for experimental treatments for TSEs to prevent deposition of abnormal PrP in the brain, because these compounds slowed the disease progression in animal disease models when administered in an earlier stage of the disease [29–33]. Reliable surrogate markers are also required to evaluate the efficacy of these experimental interventions, and [^{11}C]BF-227 PET might be one of the best candidates to assess PrP amyloid deposition in GSS. However, it remains to be elucidated if PrP amyloid levels are a particularly relevant marker of therapeutic efficacy.

A previous PET study demonstrated moderate FDDNP retention and no remarkable PIB retention in the brain of two familial CJD patients with an octapeptide repeat insertion mutation [17]. A recent PET study has additionally demonstrated no PIB retention in two autopsy-confirmed sporadic

CJD patients [18]. In contrast with these studies, the present study successfully demonstrated prominent [^{11}C]BF-227 retention in the brain of GSS patients. Differences between the previous and present findings might mainly reside in the amount and type of PrP amyloid deposits in the brain, where histopathological studies indicate higher density of PrP amyloid plaques in GSS than in familial CJD [1]. In the present study, the findings in two sporadic CJD patients showing no obvious [^{11}C]BF-227 retention in the brain additionally support this speculation. The difference may also be attributable to higher binding affinity of BF-227 to PrP amyloid cores compared to FDDNP and PIB. To clarify this, further in vitro studies comparing the binding affinities of different amyloid tracers to PrP plaques in TSE brain homogenates are needed.

The youngest GSS patient (GSS3) showed BF-227 retention in the cerebellum and thalamus but not in the neocortex. The clinical symptoms in this patient were consistent with the brain distribution of BF-227, with the patient presenting with severe gait disturbance and slurred speech resulting from cerebellar ataxia but no signs of cognitive impairment, suggesting a close relationship between PrP plaque deposition as measured by BF-227 and regional brain dysfunction. There are variations of clinical phenotypes in GSS [1, 3]. Such variations are yet to be explained; however, the pattern of regional PrP amyloid distribution might be one of the factors affecting clinical phenotypes of GSS. In vivo PrP amyloid imaging using [^{11}C]BF-227 or other PET tracers will clarify neuropathological aspects of clinical variations in GSS.

In summary, we confirmed binding of BF-227 to PrP plaques in vitro and in vivo. A clinical PET study using [^{11}C]BF-227 demonstrated in vivo detection of PrP amyloid plaques in GSS patients. This imaging technique provides a potential means of facilitating both early diagnosis and non-invasive disease monitoring of certain forms of TSEs because, despite a lack of selectivity for PrP, brain retention of BF-227 in GSS shows a distinct pattern of regional distribution than that usually observed in sporadic AD.

Acknowledgment We appreciate the assistance of Dr. S. Watanuki, Dr. M. Miyake and Dr. H. Takashima in the clinical PET studies. This study was supported in part by the Program for the Promotion of Fundamental Studies in Health Science of the NIBIO in Japan, Industrial Technology Research Grant Program of the NEDO in Japan, and Health and Labor Sciences Research Grants (Translational Research and Research on Measures for Intractable Diseases) from the Ministry of Health, Labor, and Welfare of Japan.

References

1. DeArmond SJ, Kretzschmar HA, Prusiner SB. Prion diseases. In: Graham DI, Lantos PL, editors. Greenfield's neuropathology, 7th ed. London: Hodder Arnold. p. 273–323.
2. Collins SJ, Lawson VA, Masters CL. Transmissible spongiform encephalopathies. Lancet 2004;363:51–61.
3. Collins S, McLean CA, Masters CL. Gerstmann-Sträussler-Scheinker syndrome, fatal familial insomnia, and kuru: a review of these less common human transmissible spongiform encephalopathies. J Clin Neurosci 2001;8:387–97.
4. Noguchi-Shinohara M, Hamaguchi T, Kitamoto T, Sato T, Nakamura Y, Mizusawa H, et al. Clinical features and diagnosis of dura mater graft associated Creutzfeldt Jakob disease. Neurology 2007;69:360–7.
5. Lasmézas CI, Deslys JP, Demaimay R, Adjou KT, Hauw JJ, Dormont D. Strain specific and common pathogenic events in murine models of scrapie and bovine spongiform encephalopathy. J Gen Virol 1996;77(Pt 7):1601–9.
6. Schulz-Schaeffer WJ, Tschöke S, Kranefuss N, Dröse W, Hause-Reitner D, Giese A, et al. The paraffin-embedded tissue blot detects PrP(Sc) early in the incubation time in prion diseases. Am J Pathol 2000;156:51–6.
7. Fraser JR. What is the basis of transmissible spongiform encephalopathy induced neurodegeneration and can it be repaired? Neuropathol Appl Neurobiol 2002;28:1–11.
8. Small GW, Kepe V, Ercoli LM, Siddarth P, Bookheimer SY, Miller KJ, et al. PET of brain amyloid and tau in mild cognitive impairment. N Engl J Med 2006;355:2652–63.
9. Klunk WE, Engler H, Nordberg A, Wang Y, Blomqvist G, Holt DP, et al. Imaging brain amyloid in Alzheimer's disease with Pittsburgh Compound-B. Ann Neurol 2004;55:306–19.
10. Verhoeff NP, Wilson AA, Takeshita S, Trop L, Hussey D, Singh K, et al. In-vivo imaging of Alzheimer disease beta-amyloid with [11C]SB-13 PET. Am J Geriatr Psychiatry 2004;12:584–95.
11. Rowe CC, Ackerman U, Browne W, Mulligan R, Pike KL, O'Keefe G, et al. Imaging of amyloid beta in Alzheimer's disease with 18F-BAY94–9172, a novel PET tracer: proof of mechanism. Lancet Neurol 2008;7:129–35.
12. Kudo Y, Okamura N, Furumoto S, Tashiro M, Furukawa K, Maruyama M, et al. 2-(2-[2-Dimethylaminothiazol-5-yl]ethenyl)-6-(2-[fluoro]ethoxy)benzoxazole: a novel PET agent for in vivo detection of dense amyloid plaques in Alzheimer's disease patients. J Nucl Med 2007;48:553–61.
13. Ishikawa K, Doh-ura K, Kudo Y, Nishida N, Murakami-Kubo I, Ando Y, et al. Amyloid imaging probes are useful for detection of prion plaques and treatment of transmissible spongiform encephalopathies. J Gen Virol 2004;85:1785–90.
14. Bresjanac M, Smid LM, Vovko TD, Petric A, Barrio JR, Popovic M. Molecular-imaging probe 2-(1-[6-[(2-fluoroethyl)(methyl) amino]-2-naphthyl]ethylidene) malononitrile labels prion plaques in vitro. J Neurosci 2003;23:8029–33.
15. Sadowski M, Pankiewicz J, Scholtzova H, Tsai J, Li Y, Carp RI, et al. Targeting prion amyloid deposits in vivo. J Neuropathol Exp Neurol 2004;63:775–84.
16. Hoefert VB, Aiken JM, McKenzie D, Johnson CJ. Labeling of the scrapie-associated prion protein in vitro and in vivo. Neurosci Lett 2004;371:176–80.
17. Boxer AL, Rabinovici GD, Kepe V, Goldman J, Furst AJ, Huang SC, et al. Amyloid imaging in distinguishing atypical prion disease from Alzheimer disease. Neurology 2007;69:283–90.
18. Villemagne VL, McLean CA, Reardon K, Boyd A, Lewis V, Klug G, et al. 11C-PiB PET studies in typical sporadic Creutzfeldt-Jakob disease. J Neurol Neurosurg Psychiatry 2009;80:998–1001. doi:10.1136/jnnp.2008.171496.
19. Okamura N, Suemoto T, Shimadzu H, Suzuki M, Shiomitsu T, Akatsu H, et al. Styrylbenzoxazole derivatives for in vivo imaging of amyloid plaques in the brain. J Neurosci 2004;24:2535–41.
20. Ishikawa K, Kudo Y, Nishida N, Suemoto T, Sawada T, Iwaki T, et al. Styrylbenzoazole derivatives for imaging of prion plaques and treatment of transmissible spongiform encephalopathies. J Neurochem 2006;99:198–205.

21. Waragai M, Okamura N, Furukawa K, Tashiro M, Furumoto S, Funaki Y, et al. Comparison study of amyloid PET and voxel-based morphometry analysis in mild cognitive impairment and Alzheimer's disease. J Neurol Sci 2009;285:100–8. doi:10.1016/j.jns.2009.06.005.
22. Okamura N, Furumoto S, Funaki Y, Suemoto T, Kato M, Ishikawa Y, et al. Binding and safety profile of novel benzoxazole derivative for in vivo imaging of amyloid deposits in Alzheimer's disease. Geriatr Gerontol Int 2007;7:393–400.
23. Zeidler M, Gibbs CJ Jr, Meslin F. WHO manual for strengthening diagnosis and surveillance of Creutzfeldt-Jakob disease. Geneva: World Health Organization; 1998. p. 47–51.
24. McKhann G, Drachman D, Folstein M, Katzman R, Price D, Stadlan EM. Clinical diagnosis of Alzheimer's disease: report of the NINCDS-ADRDA Work Group under the auspices of Department of Health and Human Services Task Force on Alzheimer's Disease. Neurology 1984;34:939–44.
25. Friston KJ, Holmes AP, Worsley KJ, Poline JP, Frith CD, Frackowiack RSJ. Statistical parametric maps in functional imaging: a general linear approach. Hum Brain Mapp 1995;2:189–210.
26. Masters CL, Gajdusek DC, Gibbs CJ Jr. Creutzfeldt-Jakob disease virus isolations from the Gerstmann-Sträussler syndrome with an analysis of the various forms of amyloid plaque deposition in the virus-induced spongiform encephalopathies. Brain 1981;104:559–88.
27. Ironside JW, McCardle L, Horsburgh A, Lim Z, Head MW. Pathological diagnosis of variant Creutzfeldt-Jakob disease. APMIS 2002;110:79–87.
28. Hill AF, Zeidler M, Ironside J, Collinge J. Diagnosis of new variant Creutzfeldt-Jakob disease by tonsil biopsy. Lancet 1997;349:99–100.
29. Doh-ura K, Ishikawa K, Murakami-Kubo I, Sasaki K, Mohri S, Race R, et al. Treatment of transmissible spongiform encephalopathy by intraventricular drug infusion in animal models. J Virol 2004;78:4999–5006.
30. Rainov NG, Tsuboi Y, Krolak-Salmon P, Vighetto A, Doh-Ura K. Experimental treatments for human transmissible spongiform encephalopathies: is there a role for pentosan polysulfate? Expert Opin Biol Ther 2007;7:713–26.
31. De Luigi A, Colombo L, Diomede L, Capobianco R, Mangieri M, Miccolo C, et al. The efficacy of tetracyclines in peripheral and intracerebral prion infection. PLoS One 2008;3:e1888.
32. Teruya K, Kawagoe K, Kimura T, Chen CJ, Sakasegawa Y, Doh-ura K. Amyloidophilic compounds for prion diseases. Infect Disord Drug Targets 2009;9:15–22.
33. Forloni G, Salmona M, Marcon G, Tagliavini F. Tetracyclines and prion infectivity. Infect Disord Drug Targets 2009;9:23–30.

J Neurol
DOI 10.1007/s00415-009-5396-8

ORIGINAL COMMUNICATION

Amyloid PET in mild cognitive impairment and Alzheimer's disease with BF-227: comparison to FDG–PET

Katsutoshi Furukawa · Nobuyuki Okamura · Manabu Tashiro · Masaaki Waragai · Shozo Furumoto · Ren Iwata · Kazuhiko Yanai · Yukitsuka Kudo · Hiroyuki Arai

Received: 6 June 2009 / Revised: 29 August 2009 / Accepted: 10 November 2009

Abstract We recently developed a novel PET tracer, ^{11}C-labeled 2-(2-[2-dimethylaminothiazol-5-yl]ethenyl)-6-(2-[fluoro]ethoxy)benzoxazole ([^{11}C]BF-227), and had success with in vivo detection of amyloid plaques in Alzheimer's disease (AD) brains (Kudo et al. in J Nucl Med 8:553–561, 2007). We applied this tracer to subjects with mild cognitive impairment (MCI) and AD in order to elucidate the status of amyloid plaque deposition in MCI and compared the diagnostic performance of BF-227-PET with that of FDG–PET in AD cases. We studied 12 aged normal (AN) subjects, 15 MCIs and 15 ADs with PET using [^{11}C]BF-227. PET images were obtained after administration of BF-227 and the regional standardized uptake value (SUV) and the ratio of regional to cerebellar SUV were calculated as an index of BF-227 binding. AD patients showed increased uptake of [^{11}C]BF-227 in the neocortical areas and striatum as well as decreased glucose metabolism in temporoparietal, posterior cingulate and medial temporal areas. MCI subjects showed a significant increase in BF-227 uptake in the neocortical areas similar to AD, and the most significant difference of BF-227 retention was observed in the parietal lobe if its retentions for MCI were compared to those for AD and AN. On the other hand, glucose hypometabolism in MCI was confined to cingulate and medial temporal cortices. Neocortical BF-227 uptake negatively correlated with glucose metabolism. Receiver operating characteristic (ROC) analysis indicated higher specificity and sensitivity with BF-227-PET than those with FDG–PET for differential diagnosis between AD and normal control. We conclude that [^{11}C]BF-227-PET has a possibility to be a useful technology for early detection of AD pathology and also even in the MCI stage.

Keywords Alzheimer's disease · Amyloid · Senile plaque · PET · MCI

K. Furukawa and N. Okamura equally contributed to the article.

K. Furukawa (✉) · M. Waragai · H. Arai
Department of Geriatrics and Gerontology,
Division of Brain Sciences, Institute of Development,
Aging and Cancer, Tohoku University,
4-1 Seiryomachi, Aobaku, Sendai 980-8498, Japan
e-mail: kfurukawa-ns@umin.ac.jp

N. Okamura · S. Furumoto · K. Yanai
Department of Pharmacology,
Tohoku University Graduate School of Medicine,
4-1 Seiryomachi, Aobaku, Sendai 980-8575, Japan

M. Tashiro
Division of Cyclotron Nuclear Medicine,
Cyclotron and Radioisotope Center, 6-3Aoba,
Aramaki, Aoba-ku, Sendai, Miyagi 980-8578, Japan

R. Iwata
Division of Radiopharmaceutical Chemistry,
Cyclotron and Radioisotope Center, 6-3Aoba,
Aramaki, Aoba-ku, Sendai, Miyagi 980-8578, Japan

Y. Kudo
Department of NeuroImaging Research,
Innovation New Biomedical Engineering Center,
Tohoku University, 4-1 Seiryomachi, Aobaku,
Sendai 980-8498, Japan

Introduction

Senile or amyloid plaque is a pathological hallmark of Alzheimer's disease (AD), and amyloid β peptide (Aβ), which is a main component of the senile plaque, is believed to play a key role in the pathogenesis of AD [8]. In recent years several laboratories, including ours, have succeeded in visualizing Aβ deposition in living patients' brains with

Published online: 28 November 2009

AD using PET probes [13, 14, 24]. Pittsburgh Compound-B (PIB), which is the most commonly used probe for Aβ now, has been applied not only to AD but also to several other neurological disorders [15, 24].

Petersen from the Mayo clinic addressed the concept of mild cognitive impairment (MCI), which is an intermediate state between normal aging and AD [20, 21]. The criteria he stated for MCI are cognitive concern expressed by a physician, informant, participant or nurse; cognitive impairment in one or multiple domains (executive function, memory, language or visuospatial); normal functional activities; not demented.

Regional cerebral glucose metabolism (rCMRglu) has been studied by several investigators [9, 18, 19] using [^{18}F] 2-fluoro-deoxy-D-glucose (FDG) and PET in diseases causing dementia including AD. We used BF-227-PET as well as FDG–PET on the same subjects (AN, MCI, and AD) and carefully analyzed and compared the results with these two kinds of PET. Finally using these data we investigated and compared the specificity and sensitivity of BF-227 PET and FDG–PET in diagnosing AD.

Method

Twelve ANs, 15 subjects with MCI and 15 patients with AD were recruited in the present study. The demographic information of the subjects is shown in Table 1. The diagnosis for MCI and probable AD followed the MCI clinical criteria presented by "Petersen et al." [20] and "the National Institute of Neurological and Communicative Disorders and Stroke—Alzheimer's Disease and Related Disorders Association" [17], respectively. In 15 MCI subjects, 10 were amnestic multi-domain MCI and the other 5 subjects were amnestic single-domain MCI. Mini-mental state examination (MMSE) scores were significantly different between "AN and MCI", "AN and AD", and "MCI and AD". The study protocol was approved by the Committee on Clinical Investigation at Tohoku University School of Medicine and the Advisory Committee on Radioactive Substances at Tohoku University. After a complete description of the study to the patients and subjects, written informed consent was obtained.

Table 1 Demographic details of the subjects in this study

	N	Gender	Age	MMSE
AN	12	M/F = 7/5	66.3 ± 3.3	29.9 ± 0.3
MCI	15	M/F = 8/7	78.3 ± 3.8	25.5 ± 2.5
AD	15	M/F = 5/10	72.5 ± 6.9	19.5 ± 3.7

AN aged normal, *MCI* mild cognitive impairment, *AD* Alzheimer's disease. MMSE scores are significantly different between "AN and MCI", "AN and AD", and "MCI and AD"

The PET procedure for BF-227 was described precisely before [14]. BF-227 and its *N*-desmethylated derivative (a precursor of [^{11}C]BF-227) were custom-synthesized by Tanabe R&D Service Co. [^{11}C]BF-227 was synthesized from the precursor by *N*-methylation in dimethyl sulfoxide using [^{11}C]methyl triflate. The [^{11}C]BF-227 PET study was performed using a PET SET-2400 W scanner (Shimadzu Inc., Japan). After intravenous injection of 211–366 mBq of [^{11}C]BF-227, dynamic PET images were obtained for 60 min with each subject's eyes closed. Standardized uptake value (SUV) images of [^{11}C]BF-227 were obtained by normalizing tissue radioactivity concentration by injected dose and body weight. The FDG–PET procedure was described previously [19]. Subjects were scanned in a quiet and dimly-lit room with their eyes closed after at least 4 h of food restriction. Following a 68 Ga/Ga transmission scan of 7 min duration, an emission scan, which lasted 60 min after intravenous injection of FDG, was performed. The emission data were corrected for tissue attenuation using the transmission data. Regions of interest (ROIs) were placed on individual axial magnetic resonance (MR) images in the cerebellar hemisphere, striatum, frontal, lateral temporal, medial temporal, parietal, occipital, anterior and posterior cingulate cortices. The ROI information was then copied onto dynamic PET SUV images, and regional SUVs were sampled using Dr. View/LINUX software (AJS inc., Japan). Because there were neither senile plaques nor glucose hypometabolism in the cerebellum of AD, ratios of regional SUV to cerebellar SUV (SUVR) were calculated as an index of [^{11}C]BF-227 retention and CMRglu. Neocortical SUVR was calculated by averaging SUVRs in the frontal, lateral temporal, parietal and posterior cingulate cortices.

For statistical comparison in the three groups, we applied one-way analysis of variance (ANOVA) followed by the Bonferroni-Dunn post hoc test. The performance of diagnostic indices to discriminate among groups was assessed using the ROC analysis. Areas under ROC curves (AUC) were calculated and compared using GraphPad Prism Software (GraphPad Software Inc., San Diego, CA). Statistical significance was defined as $p < 0.05$.

Results

BF-227 retention in MCI

First, we analyzed PET images with [^{11}C]BF-227 among the three groups (AN, MCI, and AD), and representative brain PET images are shown in Fig. 1. As indicated in the figure, some MCI subjects showed strong retention of [^{11}C]BF-227, but other MCI subjects did not. Most AD cases, however, indicated strong accumulation of [^{11}C]BF-227 especially in

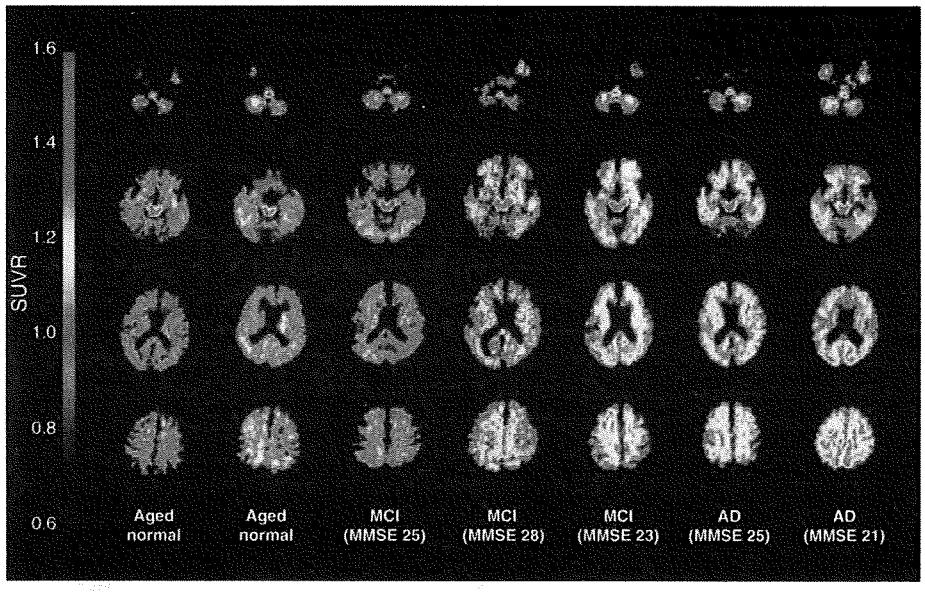

Fig. 1 Representative axial brain PET images with BF-227. Both the AD cases showed high SUVR compared to the aged normal subjects, although the MCI cases showed heterogeneity, that is, one MCI case (MMSE = 25) showed a comparative SUVR level to AN but another case showed SUVR as high as the AD level

frontal, temporal and parietal cortices. If the retention pattern of [^{11}C]BF-227 is compared to that of PIB, the accumulation of [^{11}C]BF-227 in the frontal lobe looks much weaker than that of PIB [3].

Figure 2 shows the mean neocortical and regional SUVRs of [^{11}C]BF-227 for the three groups. Both the mean neocortical SUVRs for MCI and AD are significantly higher than that for AN. As we previously reported [1], significantly higher SUVRs were observed in most cerebral regions in AD compared to AN except for the medial temporal lobe. MCI subjects indicated a significantly increased SUVR in frontal, lateral temporal, parietal, occipital cortices as well as anterior cingulate gyrus compared to AN, and the most prominent increase was observed in the lateral temporal cortex. A significantly lower SUVR in MCI was observed in the parietal cortex compared to AD. In the other neocortical regions, MCI subjects showed a tendency towards milder retention of BF-227 than that in AD. In the relationship between BF retentions and MMSE scores in all the subjects together (NC, MCI, and AD), no strong correlations were observed (data not shown).

Cerebral glucose metabolism in AN, MCI and AD

Next, we analyzed CMRglu in the same subjects using FDG–PET in order to compare to the findings with [^{11}C]BF-227, which is considered to indicate amyloid plaque depositions. As a result, a significant reduction of neocortical SUVR was observed in both MCI and AD patients compared to AN in FDG–PET (Table 1; Fig. 3). Regional SUVR in FDG–PET was significantly decreased in the cingulate gyrus and medial temporal cortex of MCI subjects and in the lateral temporal, parietal, posterior cingulate and medial temporal cortices of AD patients, compared to AN. Table 2.

Neocortical SUVR of FDG–PET for each subject was plotted against neocortical SUVR of BF-227-PET (Fig. 4a). SUVR of BF-227 negatively correlated to SUVR of FDG in analyzing the subjects from three groups all together ($r = -0.337$, $p = 0.029$). A significant correlation of regional SUVR in BF-227-PET and FDG–PET was also observed in the temporal and parietal cortices (data not shown). However, no significant correlation was observed when the analysis was confined to the subjects in each group.

Furthermore, in order to compare sensitivity and specificity to differentiate AD from AN, ROC analysis was performed for the lateral temporal SUVR of BF-227 and posterior cingulate SUVR of FDG (Fig. 4b). The AUC for BF-227 (0.994) is much higher than that for FDG (0.839), indicating that BF-227 is more sensitive as well as more specific than FDG in diagnosing AD.

Discussion

Our group recently developed a novel PET tracer, BF-227, and has reported that this compound is able to selectively detect dense amyloid deposits including senile plaques primarily in the posterior association area of AD patients. In the present study we applied this tracer to MCI cases and concluded that the mean value for the MCI cases with BF-227 was intermittent between AN and AD. Also we clarified that BF-227-PET is a useful technology to distinguish early AD patients from AN compared to FDG–PET.

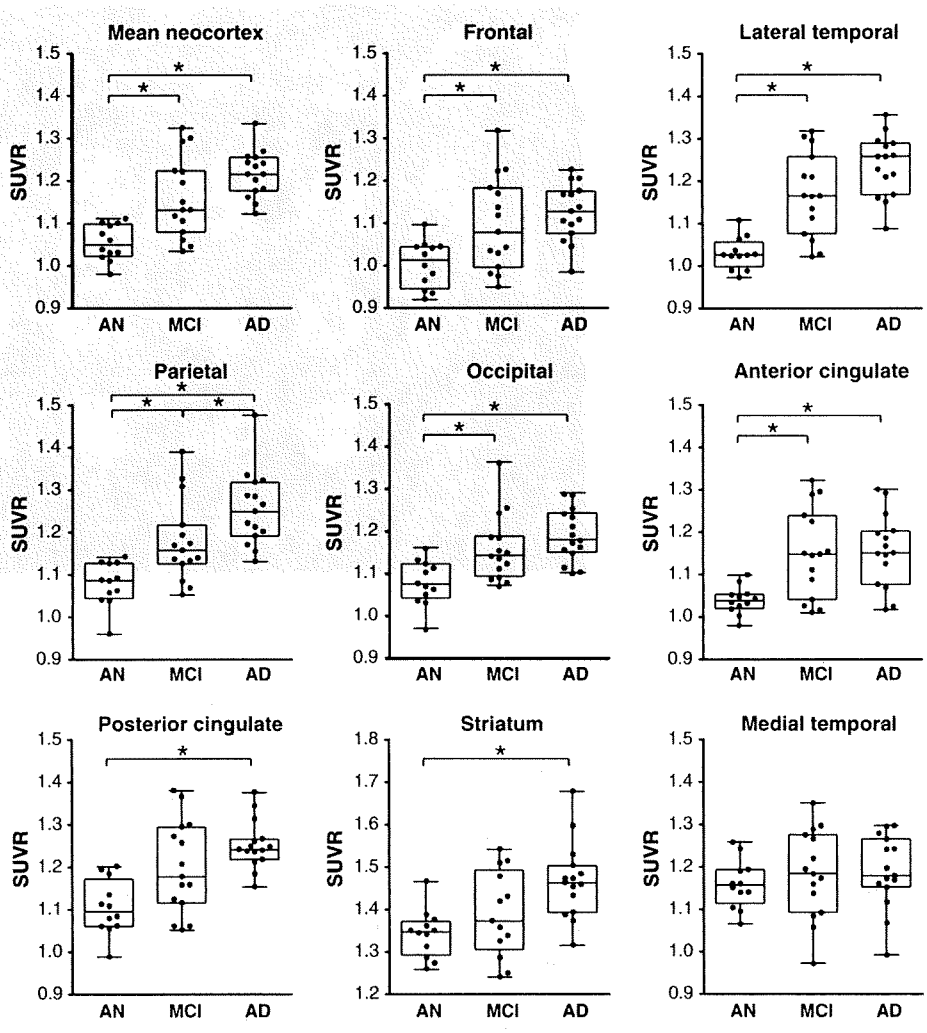

Fig. 2 Box plots of SUVR values with BF-227 PET for AN, MCI and AD. Each *dot* indicates the mean SUVR from "the mean neocortex" and "the eight regions", that is, frontal, temporal, parietal, occipital, anterior cingulate, posterior cingulated, striatum and medial temporal cortex. *Box* indicates interquartile range. *Vertical bars* indicate minimum–maximum range

MCI is now classified into 4 subtypes, that is, amnestic single-domain MCI, amnestic multi-domain MCI, non-amnestic single-domain MCI and non-amnestic multi-domain MCI. The important thing is that MCI (especially amnestic MCI) is regarded as a prodromal state of AD, in other words, a high percentage of MCI subjects are considered to convert to AD. It has been reported that 10–20% of MCI cases are going to convert to AD although only 1–2% of normal elderly convert to AD [21]. The present study concludes that MCI has high levels of [^{11}C]BF-227 retention indicating that senile plaque deposition already advances severely in the stage of MCI before dementia symptoms become obvious. Previous amyloid PET studies using ^{18}F-labeled 2-(1,1-dicyano-propen-2-yl)-6-(2-fluoroethyl)-methylamino-naphthalene (FDDNP) or PIB also indicated significant tracer retention in MCI and AD. Small et al. [24] presented that FDDNP can detect a high signal in MCI by binding not only for amyloid plaques but also tau neurofibrillary tangles, and the retention level for MCI is between AN and AD. On the other hand, several groups reported that about a half of the MCI subjects showed PIB uptake in the AD range, and other MCI subjects indicated retention levels lower than the AD range [12]. A group from Sweden concluded that MCI subjects who converted to AD later showed significantly higher PIB retention compared to non-converting MCI subjects and NC [6]. The present study also revealed higher retention of BF-227 in 60–70% of MCI subjects and in almost all the AD patients. Therefore, the amyloid PET technique is considered to be a highly useful and strong method for early detection of AD patients in the MCI stage. These pieces of information are indispensable in applying new treatment technologies against dementia into the prodromal stage of Alzheimer's disease. In other words, because it is considered that aggregation and deposition of Aβ starts much earlier before patients indicate symptoms of dementia, it is undoubtedly important to detect Aβ deposition as early as

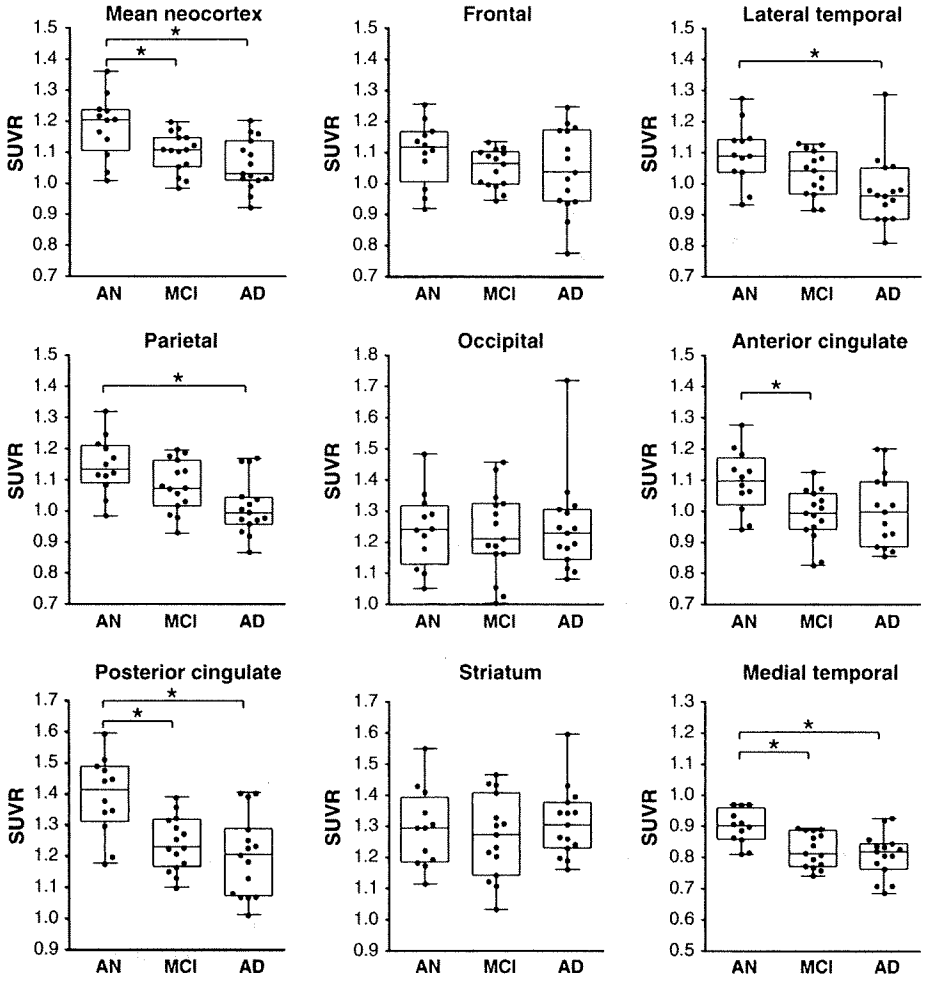

Fig. 3 Box plots of SUVR values with FDG–PET for AN, MCI and AD. Each *dot* indicates the mean SUVR from the mean neocortex and eight cerebral regions, that is, frontal, temporal, parietal, occipital, anterior cingulate, posterior cingulated, striatum and medial temporal cortex. *Boxes* indicate interquartile range. *Vertical bars* indicate minimum–maximum range

Table 2 Comparison of SUVR values of BF-227-PET and FDG–PET

		Mean neo cortex	Frontal	Lateral temporal	Parietal	Occipital	Anterior cingulate	Posterior cingulate	Striatum	Medial temporal
BF-227	AN	1.05 ± 0.04	1.00 ± 0.06	1.03 ± 0.04	1.08 ± 0.05	1.08 ± 0.05	1.04 ± 0.03	1.11 ± 0.07	1.34 ± 0.06	1.16 ± 0.06
	MCI	1.16 ± 0.10*	1.10 ± 0.11*	1.17 ± 0.10*	1.18 ± 0.10*	1.16 ± 0.08*	1.15 ± 0.11*	1.20 ± 0.11	1.41 ± 0.11	1.18 ± 0.10
	AD	1.22 ± 0.06*	1.13 ± 0.07*	1.24 ± 0.07*	1.25 ± 0.09*†	1.19 ± 0.06*	1.16 ± 0.09*	1.25 ± 0.06*	1.47 ± 0.09*	1.19 ± 0.09
FDG	AN	1.18 ± 0.10	1.10 ± 0.11	1.10 ± 0.10	1.15 ± 0.09	1.24 ± 0.12	1.10 ± 0.10	1.39 ± 0.13	1.29 ± 0.13	0.90 ± 0.06
	MCI	1.10 ± 0.06*	1.05 ± 0.06	1.03 ± 0.07	1.08 ± 0.08	1.23 ± 0.14	0.99 ± 0.08*	1.24 ± 0.09*	1.27 ± 0.13	0.82 ± 0.06*
	AD	1.06 ± 0.08*	1.05 ± 0.14	0.98 ± 0.11*	1.01 ± 0.09*	1.25 ± 0.15	1.00 ± 0.12	1.20 ± 0.13*	1.31 ± 0.11	0.81 ± 0.07*

Mean SUVR value for each brain region was obtained from AN, MCI and AD. * $p < 0.05$, versus AN, † $p < 0.05$ versus MCI

possible in order to begin medication to prevent or treat cognitive decline before the manifestations of dementia become clear.

In most PIB positive MCI and AD cases presented by several different laboratories, the frontal cortex showed high PIB retention, although the frontal cortex is not a region where amyloid plaques are predominantly rich in the early stage of AD or MCI according to the autopsy studies [1, 10]. Our newly developed tracer, BF-227, showed relatively high retention in temporal and parietal lobes for MCI and AD compared to the results with PIB. Since it is well known that the functional activity of the parietal lobe decreases in the early stage of AD [16], it is reasonable that the distribution of high BF-227-PET

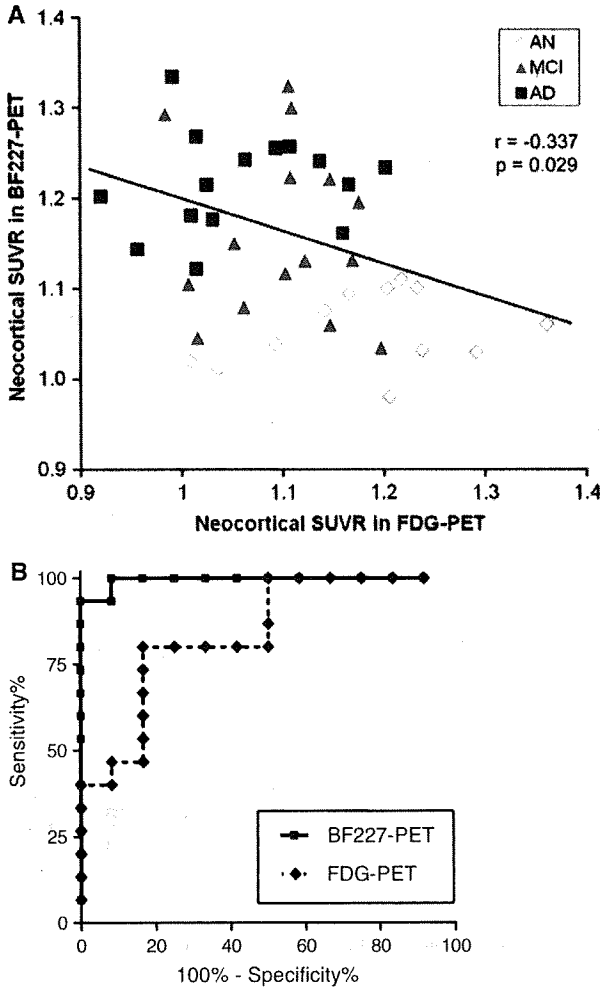

Fig. 4 **a** Relationship between neocortical SUVRs in FDG–PET and BF-227-PET. Neocortical SUVR of FDG–PET for each subject was plotted against neocortical SUVR of BF-227-PET. White, gray and black dots indicate AN, MCI and AD, respectively. **b** Receiver operating characteristic (ROC) curves of BF-227 and FDG–PET. BF-227-PET SUVR in the lateral temporal cortex and FDG–PET SUVR in the posterior cingulate cortex for differentiation between AD and AN

retention is closely related to the area indicating functional deterioration in the early stage of AD or MCI.

Low rCMRglu in AD especially in the posterior cingulate, precuneus, temporoparietal and frontal cortices was reported. FDG–PET has also been used in investigations for MCI, and low rCMRglu in the temporo-parietal and medial frontal cortices and hippocampus was reported as the most prominent predictor of subsequent cognitive decline [2–5]. Our results indicate, however, that amyloid retention detected by BF-227 is more sensitive and specific than FDG–PET for AD diagnosis. Therefore it is reasonable that amyloid PET is more sensitive than FDG–PET for detecting MCI, which is regarded as a prodromal state of dementia or early AD. According to previous autopsy studies with MCI, amyloid plaques were found predominantly in the temporal lobe structure and most amnestic MCI cases showed Braak stage II or III [11, 22]. Furthermore both neurofibrillary tangles and senile plaques were found in nondemented aging and "preclinical" AD, and profound neuronal loss was observed in layer II of the entorhinal cortex [7, 23]. Our results with BF-227 PET for MCI presented here agree with postmortem studies because BF-227 also showed high retention predominantly in the temporal lobe and the retention was intermittent between NC and AD. There are some discrepancies, however, between the results with our BF-227-PET and with autopsy, that is, some cerebral white matter, thalamus and pons showed high retention of BF-227 in MCI, although these regions are usually not rich in senile plaques in the autopsy studies. Although it is considered that the deposition of BF-227 in these regions comes from its non-specific retention by high lipophilicity, it is supposed that more precise studies are needed using more subjects for both PET and autopsy.

We now have to carefully consider the heterogeneity of BF-227 retention in MCI, which was also observed in FDDNP or PIB studies, that is, some subjects show rich retention but others do not. Although it was reported that MCI subjects showing high retention of PIB had a high tendency to convert to AD as we mentioned above [6], the number of subjects they examined was relatively small. Therefore, further careful studies are needed to clarify if the accumulation of amyloid PET probes correlates with the severity of cognitive impairment and a conversion rate to dementia.

Our results using BF-227 for MCI are "continuous" rather than "off/on", "negative/positive" or "dichotomous" signals compared to those with PIB. We speculate that because BF-227 can depict a small difference of amyloid deposition more finely than PIB, the results with BF-227 in MCI are more continuous than those with PIB. Therefore, BF-227 could reveal a degree of senile plaque deposition more precisely and accurately than PIB as far as in cases with MCI.

We would like to conclude that our newly developed amyloid PET tracer, BF-227, can detect amyloid aggregation and deposition in MCI cases and the PET signal intensity for MCI was intermittent between NC and AD. Results obtained with BF-227 PET are significantly more sensitive and specific than FDG–PET in diagnosing AD. As far as the retention pattern in the frontal and parietal cortices, BF-227 more accurately reflects senile plaque deposition observed in the autopsy studies than PIB does. Therefore, BF-227 PET should be an invaluable tool for diagnosis of AD in the early stage. Finally, we recently developed a novel probe, which has similar structure to BF-

227, labeled with F-18, and applied it to living humans. We have finished more than 20 cases so far and obtained similar results to BF-227.

Acknowledgments This study was supported by the Program for the Promotion of Fundamental Studies in Health Science by the National Institute of Biomedical Innovation, the Special Coordination Funds for Promoting Science and Technology, the Industrial Technology Research Grant Program from the New Energy and Industrial Technology Development Organization of Japan, Health and Labour Sciences Research Grants for Translational Research from the Ministry of Health, and the Ministry of Education, Culture, Sports and Technology. We appreciate technical assistance of Dr. Shoichi Watanuki and Dr. Yoichi Ishikawa in the clinical PET studies and Dr. Motohisa Kato in the imaging analysis.

References

1. Bennett DA, Cochran EJ, Saper CB, Leverenz JB, Gilley DW, Wilson RS (1993) Pathological changes in frontal cortex from biopsy to autopsy in Alzheimer's disease. Neurobiol Aging 14:589–596
2. Chételat G, Desgranges B, de la Sayette V, Viader F, Eustache F, Baron JC (2003) Mild cognitive impairment: Can FDG-PET predict who is to rapidly convert to Alzheimer's disease? Neurology 60:1374–1377
3. Chételat G, Eustache F, Viader F, De La Sayette V, Pélerin A, Mézenge F, Hannequin D, Dupuy B, Baron JC, Desgranges B (2005) FDG–PET measurement is more accurate than neuropsychological assessments to predict global cognitive deterioration in patients with mild cognitive impairment. Neurocase 11:14–25
4. de Leon MJ, Convit A, Wolf OT, Tarshish CY, DeSanti S, Rusinek H, Tsui W, Kandil E, Scherer AJ, Roche A, Imossi A, Thorn E, Bobinski M, Caraos C, Lesbre P, Schlyer D, Poirier J, Reisberg B (2001) Fowler et al. Prediction of cognitive decline in normal elderly subjects with 2-[(18)F]fluoro-2-deoxy-D-glucose/positron-emission tomography (FDG/PET). Proc Natl Acad Sci USA 98:10966–10971
5. Drzezga A, Lautenschlager N, Siebner H, Riemenschneider M, Willoch F, Minoshima S, Schwaiger M, Kurz A (2003) Cerebral metabolic changes accompanying conversion of mild cognitive impairment into Alzheimer's disease: a PET follow-up study. Eur J Nucl Med Mol Imaging 30:1104–1113
6. Forsberg A, Engler H, Almkvist O, Blomquist G, Hagman G, Wall A, Ringheim A, Långström B, Nordberg A (2008) A PET imaging of amyloid deposition in patients with mild cognitive impairment. Neurobiol Aging 29:1456–1465
7. Gómez-Isla T, Price JL, McKeel DW Jr, Morris JC, Growdon JH, Hyman BT (1996) Profound loss of layer II entorhinal cortex neurons occurs in very mild Alzheimer's disease. J Neurosci 16:4491–4500
8. Hardy J, Selkoe DJ (2002) The amyloid hypothesis of Alzheimer's disease: progress and problems on the road to therapeutics. Science 297:353–356
9. Herholz K, Carter SF, Jones M (2007) PET studies in dementia. Br J Radiol 80:S160–S167
10. Iwatsubo T, Odaka A, Suzuki N, Mizusawa H, Nukina N, Ihara Y (1994) Visualization of A beta 42(43) and A beta 40 in senile plaques with end-specific A beta monoclonals: evidence that an initially deposited species is A beta 42(43). Neuron 13:45–53
11. Jicha GA, Parisi JE, Dickson DW, Johnson K, Cha R, Ivnik RJ, Tangalos EG, Boeve BF, Knopman DS, Braak H, Petersen RC (2006) Neuropathologic outcome of mild cognitive impairment following progression to clinical dementia. Arch Neurol 63:674–681
12. Kemppainen NM, Aalto S, Wilson IA, Någren K, Helin S, Brück A, Oikonen V, Kailajärvi M, Scheinin M, Viitanen M, Parkkola R, Rinne JO (2007) PET amyloid ligand [11C]PIB uptake is increased in mild cognitive impairment. Neurology 68:1603–1606
13. Klunk WE, Engler H, Nordberg A, Wang Y, Blomqvist G, Holt DP, Bergström M, Savitcheva I, Huang GF, Estrada S, Ausén B, Debnath ML, Barletta J, Price JC, Sandell J, Lopresti BJ, Wall A, Koivisto P, Antoni G, Mathis CA, Långström B (2004) Imaging brain amyloid in Alzheimer's disease with Pittsburgh Compound-B. Ann Neurol 55:306–319
14. Kudo Y, Okamura N, Furumoto S, Tashiro M, Furukawa K, Maruyama M, Itoh M, Iwata R, Yanai K, Arai H (2007) 2-(2-[2-Dimethylaminothiazol-5-yl]ethenyl) -6-(2-[fluoro]ethoxy)benzoxazole: a novel PET agent for in vivo detection of dense amyloid plaques in Alzheimer's disease patients. J Nucl Med 8:553–561
15. Mathis CA, Klunk WE, Price JC, DeKosky ST (2005) Imaging technology for neurodegenerative diseases: progress toward detection of specific pathologies. Arch Neurol 62:196–200
16. Matsuda H (2007) Role of neuroimaging in Alzheimer's disease, with emphasis on brain perfusion SPECT. J Nucl Med 48:1289–1300
17. McKhann G, Drachman D, Folstein M, Katzman R, Price D, Stadlan EM (1984) Clinical diagnosis of Alzheimer's disease: report of the NINCDS-ADRDA Work Group under the auspices of Department of Health and Human Services Task Force on Alzheimer's Disease. Neurology 34:939–944
18. Minoshima S, Giordani B, Berent S, Frey KA, Foster NL, Kuhl DE (1997) Metabolic reduction in the posterior cingulate cortex in very early Alzheimer's disease. Ann Neurol 42:85–94
19. Okamura N, Arai H, Higuchi M, Tashiro M, Matsui T, Hu XS, Takeda A, Itoh M, Sasaki H (2001) [18F]FDG–PET study in dementia with Lewy bodies and Alzheimer's disease. Prog Neuropsychopharmacol Biol Psychiatry 25:447–456
20. Petersen RC, Smith GE, Waring SC, Ivnik RJ, Tangalos EG, Kokmen E (1999) Mild cognitive impairment: clinical characterization and outcome. Arch Neurol 56:303–308
21. Petersen RC (2004) Mild cognitive impairment as a diagnostic entity. J Intern Med 256:183–194
22. Petersen RC, Parisi JE, Dickson DW, Johnson K, Cha R, Ivnik RJ, Tangalos EG, Boeve BF, Knopman DS, Braak H, Petersen RC (2006) Neuropathologic features of amnestic mild cognitive impairment. Arch Neurol 63:665–672
23. Price JL, Morris JC (1999) Tangles and plaques in nondemented aging and "preclinical" Alzheimer's disease. Ann Neurol 45:358–368
24. Small GW, Kepe V, Ercoli LM, Siddarth P, Bookheimer SY, Miller KJ, Lavretsky H, Burggren AC, Cole GM, Vinters HV, Thompson PM, Huang SC, Satyamurthy N, Phelps ME, Barrio JR (2006) PET of brain amyloid and tau in mild cognitive impairment. N Engl J Med 355:2652–2663

Journal of the Neurological Sciences xxx (2009) xxx–xxx

Contents lists available at ScienceDirect

Journal of the Neurological Sciences

journal homepage: www.elsevier.com/locate/jns

Comparison study of amyloid PET and voxel-based morphometry analysis in mild cognitive impairment and Alzheimer's disease

Masaaki Waragai [a], Nobuyuki Okamura [b,*], Katsutoshi Furukawa [a], Manabu Tashiro [c], Shozo Furumoto [b,d], Yoshihito Funaki [e], Motohisa Kato [b], Ren Iwata [e], Kazuhiko Yanai [b], Yukitsuka Kudo [f], Hiroyuki Arai [a]

[a] Department of Geriatrics and Gerontology, Division of Brain Sciences, Institute of Development, Aging and Cancer, Tohoku University, Sendai, Japan
[b] Department of Pharmacology, Tohoku University School of Medicine, Sendai, Japan
[c] Division of Cyclotron Nuclear Medicine, Cyclotron and Radioisotope Center, Tohoku University, Sendai, Japan
[d] Department of Nuclear Medicine and Radiology, Institute of Development, Aging and Cancer, Tohoku University, Sendai, Japan
[e] Division of Radiopharmaceutical Chemistry, Cyclotron and Radioisotope Center, Tohoku University, Sendai, Japan
[f] Innovation of New Biomedical Engineering Center, Tohoku University, Sendai, Japan

ARTICLE INFO

Article history:
Received 27 February 2009
Received in revised form 5 May 2009
Accepted 2 June 2009
Available online xxxx

Keywords:
Alzheimer's disease
Amyloid
Early diagnosis
Magnetic resonance imaging
Positron emission tomography
BF-227

ABSTRACT

Two techniques employed for the early diagnosis of dementia are the imaging of amyloid-β protein using positron emission tomography (PET) and voxel-based morphometry analysis of MRI (VBM-MRI). The purpose of this study was to evaluate the clinical utility of amyloid PET and VBM-MRI for the early diagnosis and tracking of the severity of Alzheimer's disease (AD). The neuritic plaque burden and gray matter losses were evaluated using [^{11}C]BF-227-PET and VBM-MRI in 12 healthy controls, 13 subjects with mild cognitive impairment (MCI), including 6 who converted to AD and 7 who did not convert, and 15 AD patients. The AD patients and the MCI converters exhibited a neocortical retention of BF-227 and parahippocampal gray matter loss shown by VBM-MRI. The MCI converters were more clearly distinguished from the MCI non-converters in BF-227-PET than VBM-MRI. The combined sample of the MCI converters and AD patients showed a significant correlation of MMSE scores with the global gray matter loss, but not with the BF-227 retention. These findings suggest that amyloid PET using [^{11}C]BF-227 is better suited for the prediction of conversion from MCI to AD, while VBM-MRI appears to be better suited for tracking the severity of dementia.

1. Introduction

Alzheimer's disease (AD) is a neurodegenerative disorder characterized by a progressive impairment of cognitive function and behavior. AD is the most common form of dementia, particularly in the elderly [1,2]. The pathological hallmarks of AD are extracellular amyloid-β protein deposits called senile plaques (SPs) and intracellular neurofibrillary tangles (NFTs), which occur together with selective neuronal and synaptic loss [3,4]. These changes are also associated with progressive neuronal loss and resultant cerebral atrophy [5]. The presence of both SPs and NFTs are prerequisites for a definitive diagnosis of AD, but more attention has been focused on the role of amyloid-β protein (Aβ) in the pathogenesis of AD. Although the mechanisms of development of AD have not been completely elucidated, Aβ is assumed to play a causal role in the pathology of AD.

In vivo imaging techniques that can non-invasively and reliably assess Aβ deposition are currently receiving considerable attention in the search for a method for early diagnosis of AD [6–11]. Pittsburgh Compound-B (PIB) is at present the most commonly used probe for Aβ and has been applied to the diagnosis of AD and several other neurological disorders [12–16]. For example, amnesic mild cognitive impairment (MCI) is currently considered a prodromal state of AD, though not all individuals with MCI will develop AD; MCI converters and non-converters are difficult to distinguish from a clinical and neuropsychological perspective. Analysis of PIB-PET images in MCI subjects revealed a bimodal distribution of PIB uptake in the neocortex. About two thirds of MCI cases showed neocortical retention of PIB similar in distribution (and sometimes in degree) to AD, while the other third of MCI cases showed no cortical retention, similar to normal individuals [15,17,18]. A previous PIB-PET study demonstrated higher PIB retention in MCI converters than in non-converters, suggesting the utility of amyloid imaging in the prediction of progression to dementia [18].

We have developed novel benzoxazole derivatives for in vivo imaging of amyloid [19–21]. One of these agents, 2-(2-[2-demethylaminothiazol-5-yl]ethenyl)-6-(2-[Fluoro]ethoxy)benzoxazole (BF-227), displayed a high binding affinity to Aβ fibrils, excellent brain uptake and specifically labels amyloid deposits in transgenic mice [20,22]. A clinical PET study using [^{11}C]BF-227 demonstrated higher retention of this tracer in the

* Corresponding author. Department of Pharmacology, Tohoku University School of Medicine, Tohoku University, 2-1 Seiryo-machi, Aoba-ku, Sendai 980-8575, Japan. Tel.: +81 22 717 8058; fax: +81 22 717 8060.
E-mail address: oka@mail.tains.tohoku.ac.jp (N. Okamura).

0022-510X/$ - see front matter © 2009 Elsevier B.V. All rights reserved.
doi:10.1016/j.jns.2009.06.005

Please cite this article as: Waragai M, et al, Comparison study of amyloid PET and voxel-based morphometry analysis in mild cognitive impairment and Alzheimer's disease, J Neurol Sci (2009), doi:10.1016/j.jns.2009.06.005